- Supplementary Information –

First Comparative Study of the Three Polymorphs of Bis(isonicotinamide) Citric Acid Cocrystals and the Concomitant Salt 4-carbamoylpyridinium Citrate Isonicotinamide

Paul Stainton[§], Tudor Grecu[†], Jim McCabe[†], Tasnim Munshi[‡], Elisa Nauha[‡], Ian J. Scowen[‡], Nicholas Blagden[§].*

[§]School of Pharmacy, University of Lincoln, LN6 7TS, UK.
[†]Pharmaceutical Sciences, IMED, AstraZeneca, Macclesfield, SK10 2NA, UK.
[‡]School of Chemistry, University of Lincoln, LN6 7TS, UK.
[*]email: nblagden@lincoln.ac.uk

Content:

1. Supporting Powder Pattern Indexing

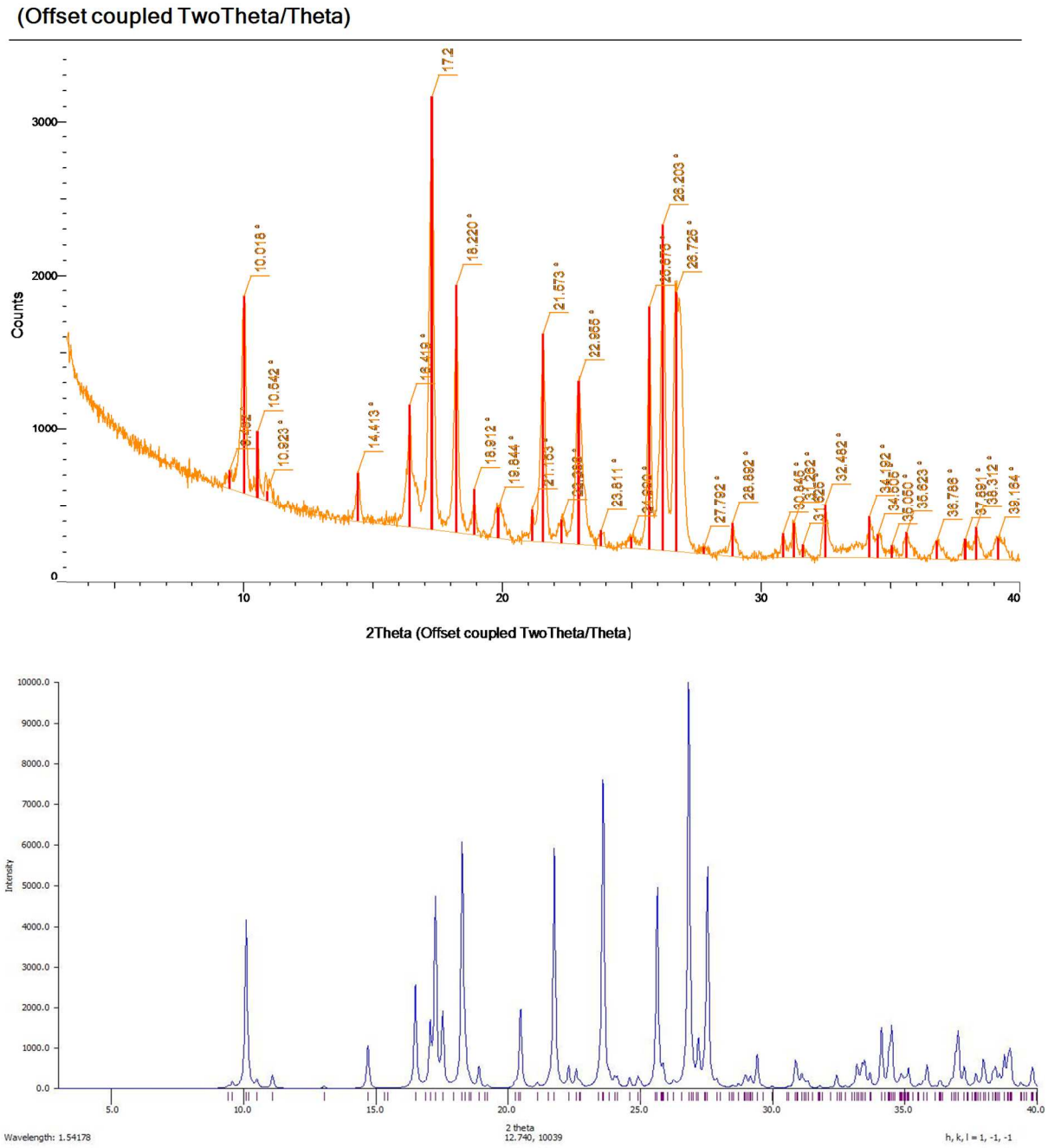

Figure S1 – Experimental (top) and simulated (bottom) powder pattern of α form.

Table S1 - Peak List Comparing Simulated to Actual Powder Patterns – α Form.

Simulated Peak	Counts	Actual Peak	(hkl)
9.556	135	9.402	(001)
10.126	4151	10.018	(100)
10.5	232	10.542	(1-10)
11.091	309	10.923	(01-1)
13.051	38		(1-1-1)
14.701	1042	14.413	(11-1)
16.505	2568	16.419	(110)
17.066	1680		(10-2)
17.252	4768	17.2	(1-20)
17.532	1892		(2-1-1)
18.248	6062	18.22	(02-1)
18.933	541	18.912	(020)
20.458	1950		(20-2)
21.733	5927	21.573	(2-2-1)
22.294	560	22.288	(02-2)
22.574	483	22.995	(12-1)
23.601	7568	23.881	(21-2)
24.596	270		(2-21)
24.939	290	24.999	(1-22)
25.654	4961	25.675	(102)
26.837	9981	26.725	(3-1-2)
27.21	1255		(3-2-1)
27.553	5483	27.792	(30-2)
28.984	328	28.892	(003)
29.171	328		(02-3)
29.42	830		(3-2-2)
30.882	695	30.845	(112)
31.131	386	31.282	(2-12)
32.407	328	32.482	(22-3)
33.185	598		(2-2-3)
33.465	695		(31-3)
33.683	386		(2-32)
34.119	1486	34.192	(202)
34.492	1544	34.505	(20-4)
35.146	502	35.05	(1-40)
35.861	598		(310)
37.013	1409		(01-4)
37.977	714	37.891	(3-1-4)
38.973	985		(32-1)

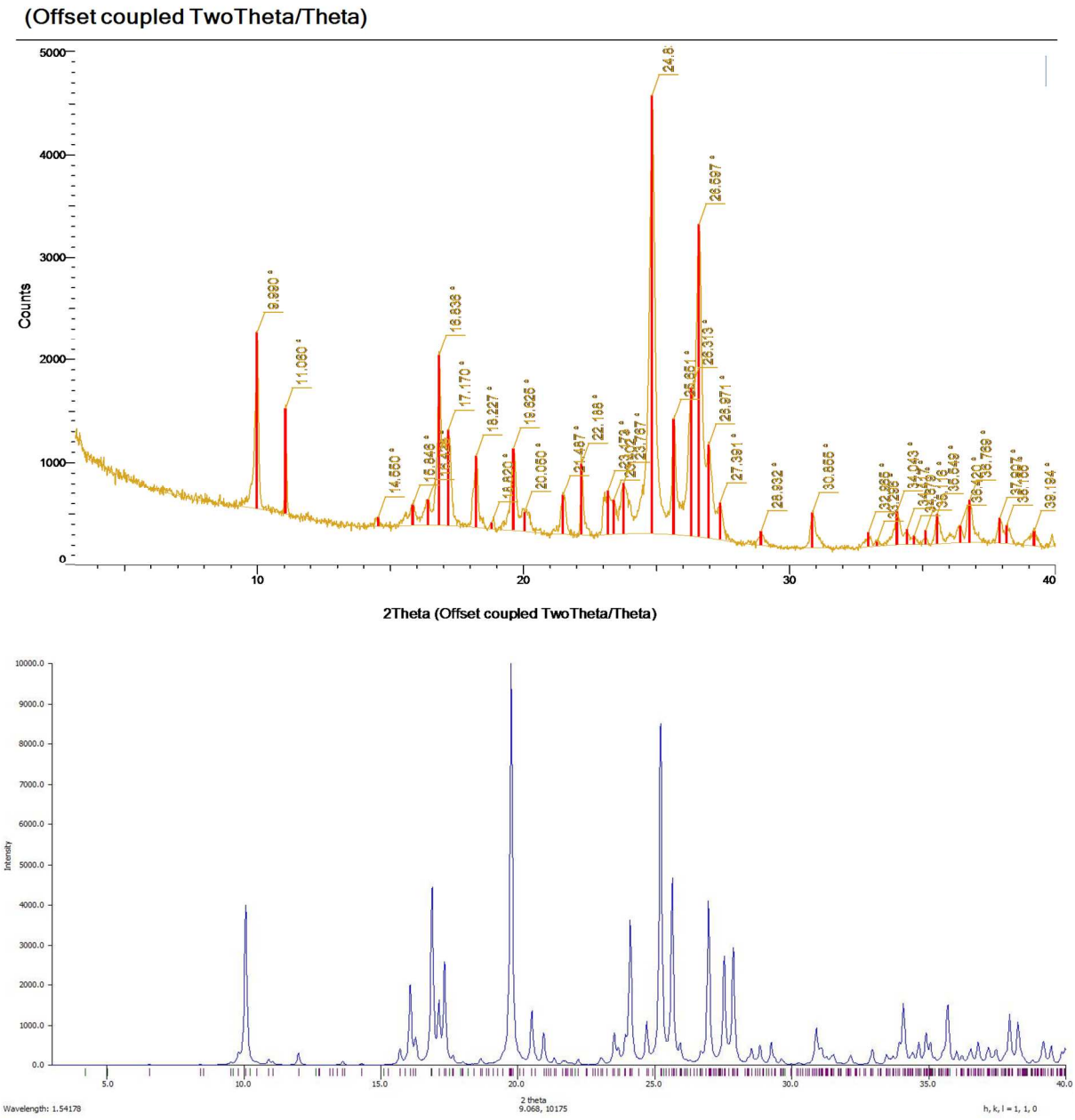

Figure S2 – Experimental (top) and simulated (bottom) powder pattern of β form.

Table S2 - Peak List Comparing Simulated to Actual Powder Patterns – β Form.

Simulated Peak	Counts	Actual Peak	(hkl)
10.066	4011	9.99	(002)
12.007	263		(120)
15.702	403	15.848	(013)
16.079	1996		(122)
16.888	4448	16.836	(040)
17.131	1646	17.17	(200)
17.32	2609		(023)
19.747	10000	19.625	(033)
20.529	1366		(202)
20.934	823		(212)
23.523	841	23.402	(151)
24.089	3660		(124)
24.709	1121	24.8	(143)
25.222	8546		(223)
25.653	4694	25.651	(20-4)
26.974	4081	26.971	(233)
27.541	2750		(204)
27.864	2925		(214)
28.539	420		(16-2)
28.835	473	28.932	(224)
29.24	560		(243)
30.912	928	30.855	(22-5)
32.934	385	32.955	(32-4)
34.094	1541	34.043	(20-6)
34.93	823	34.879	(41-1)
35.685	1524	35.549	(27-2)
36.818	578	36.769	(16-5)
37.95	1278	37.997	(42-3)
38.247	1086	38.166	(24-6)
39.191	613	39.194	(34-5)
39.488	438		(44-2)

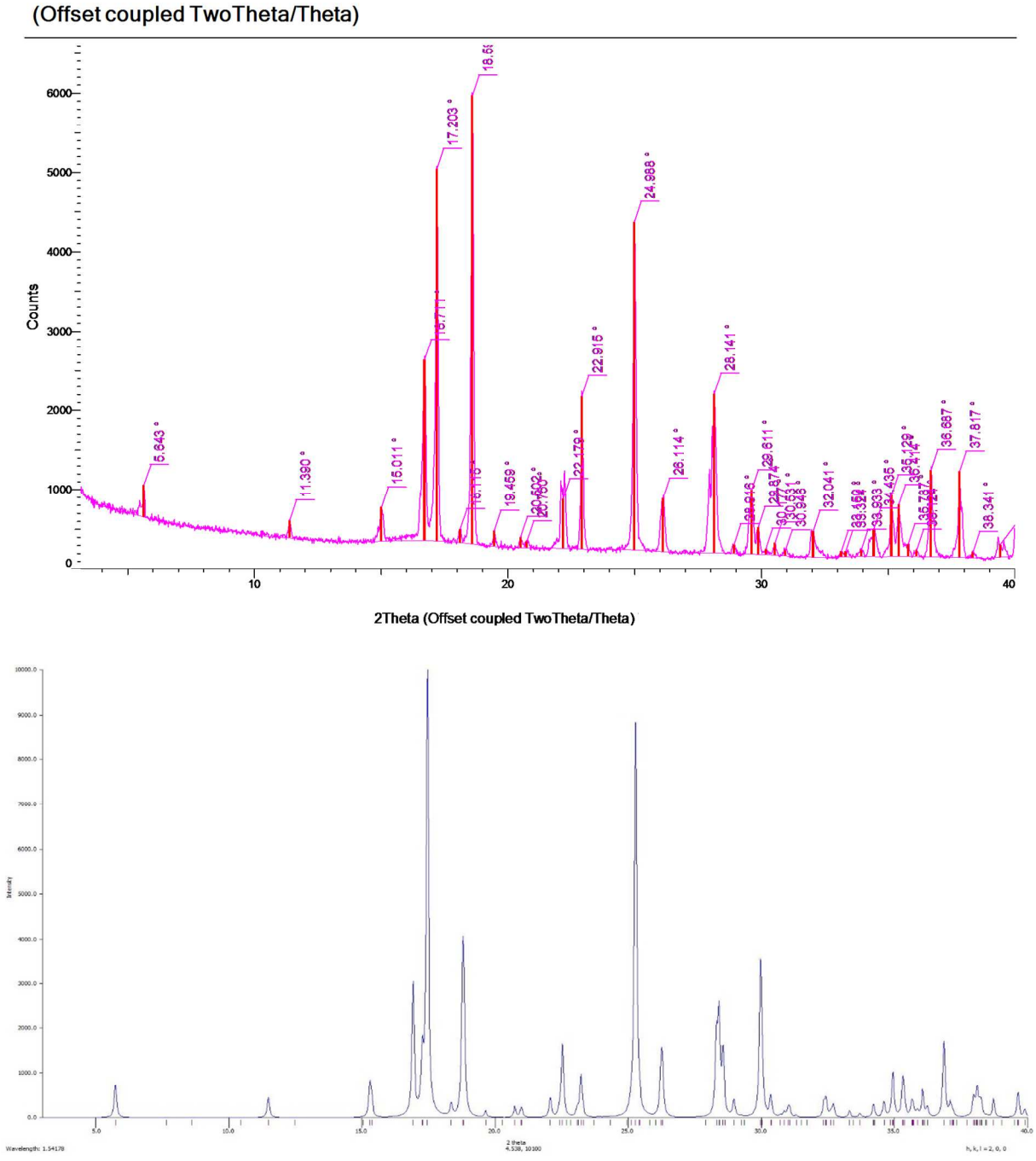

Figure S3 – Experimental (top) and simulated (bottom) powder pattern of γ form.

Table S3 - Peak List Comparing Simulated to Actual Powder Patterns – γ Form.

Simulated Peak	Counts	Actual Peak	(hkl)
5.744	725	5.643	(200)
11.502	446	11.39	(400)
15.306	882	15.011	(20-2)
16.927	3047	16.711	(110)
17.488	10000	17.203	(202)
18.361	357	18.115	(11-1)
18.819	4074	18.59	(111)
19.65	156	19.459	(31-1)
20.731	246	20.502	(60-2)
21.001	234	20.76	(402)
22.082	446		(510)
22.539	1674	22.179	(11-2)
23.225	971	22.915	(31-2)
25.283	8850	24.988	(51-2)
26.26	1574	26.114	(710)
28.401	2612	28.141	(71-2)
28.567	1641		(31-3)
28.983	391	28.916	(100)
29.981	3549	29.611	(51-3)
30.355	525	30.177	(802)
32.413	469	32.041	(71-3)
34.949	1016	34.435	(80-4)
35.323	971	35.129	(404)
36.051	625		(114)
36.861	1730	36.687	(11 1-2)
38.108	725	37.817	(42-2)
38.711	435	38.341	(604)
39.667	547	39.5	(621)

The simulated peaks match very closely to the actual but they are all shifted down by approximately 0.2-0.3 due to the temperature difference. Despite the shift all the peaks are present, it is certain that the sample was purely polymorph 3.

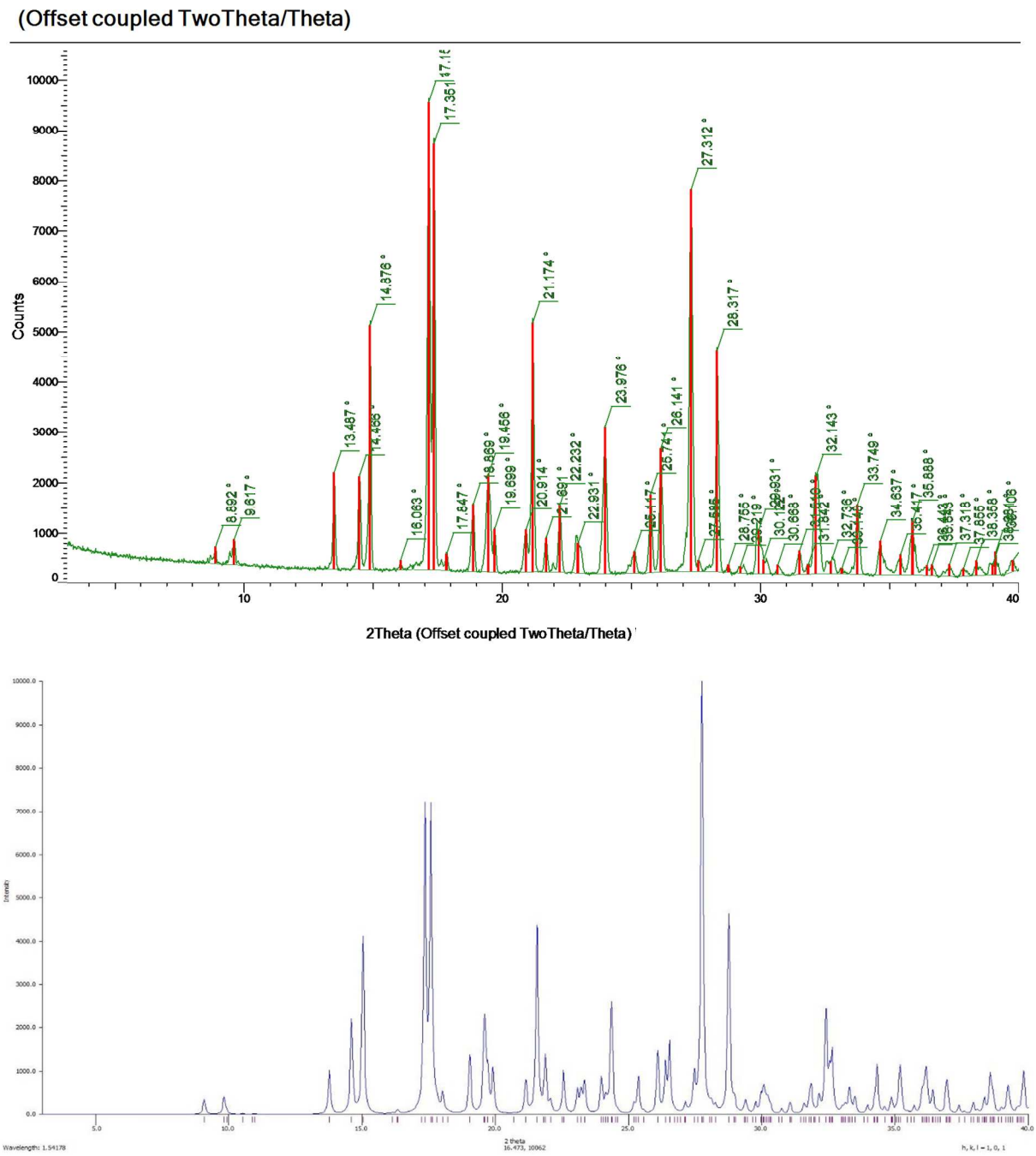

Figure S4 – Experimental (top) and simulated (bottom) powder pattern of salt form.

Table S4 - Peak List Comparing Simulated to Actual Powder Patterns – Salt Form.

Simulated Peak	Counts	Actual Peak	(hkl)
9.099	338	8.892	(001)
9.837	375	9.617	(01-1)
13.769	1038	13.487	(1-11)
14.618	2225	14.466	(1-1-1)
15.043	4100	14.876	(11-1)
17.367	7238	17.18	(110)
17.59	7238	17.351	(02-1)
19.065	1375	18.869	(2-10)
19.601	2312	19.456	(2-1-1)
19.914	1100	19.699	(020)
21.165	825	20.931	(200)
21.589	4375	21.174	(1-22)
21.88	1388	21.691	(2-20)
22.572	1025	22.232	(2-11)
23.377	800	22.931	(111)
23.98	862		(2-1-2)
24.382	2625	23.976	(01-3)
25.388	888	25.117	(10-3)
26.103	1450	25.741	(201)
26.55	1712	26.141	(1-32)
27.778	10000	27.312	(2-31)
28.761	4650	28.317	(2-12)
30.08	700	29.931	(3-1-2)
31.845	712	31.51	(11-4)
32.426	2450	32.143	(13-1)
34.325	1175		(2-23)
35.196	1150	34.637	(31-3)
36.179	1112	35.888	(130)
36.961	800		(1-40)
38.592	962	38.358	(2-1-4)
39.24	700		(1-1-4)
39.844	1012		(4-2-2)

The simulated peaks match very closely to the actual except they all seem to be shifted down by approximately 0.2-0.3. Despite the shift all the peaks are present with the addition of one peak at 33.749 which may be present in P1 but due to other notable peaks for P1 being absent that the sample was purely polymorph 4.

2. Supporting Single Crystal Analysis

Table S5 - Crystal Structure of α Form.

Crystal data

$C_6H_8O_7 \cdot 2(C_6H_6N_2O)$	$F(000) = 456$
$M_r = 436.38$	
Triclinic, P	$D_x = 1.513$ Mg m^{-3}
$a = 10.4670$ (4) Å	Cu $K\alpha$ radiation, $\lambda = 1.54178$ Å
$b = 10.4844$ (4) Å	Cell parameters from 9916 reflections
$c = 10.5487$ (4) Å	$\theta = 4.7–72.2°$
$\alpha = 98.7808$ (11)°	$\mu = 1.06$ mm^{-1}
$\beta = 112.535$ (1)°	$T = 173$ K
$\gamma = 109.0792$ (12)°	Block, colourless
$V = 957.90$ (6) Å^3	0.36 × 0.24 × 0.12 mm
$Z = 2$	

Data collection

Bruker D8 Venture Photon diffractometer	3598 reflections with $I > 2\sigma(I)$
Radiation source: IμS Cu	$R_{int} = 0.023$
	$\theta_{max} = 72.2°$, $\theta_{min} = 4.7°$
φ and ω scans	$h = -12 \quad 12$
Absorption correction: multi-scan SADABS 2016/2: Krause, L., Herbst-Irmer, R., Sheldrick G.M. & Stalke D., J. Appl. Cryst. 48 (2015) 3-10	$k = -12 \quad 12$
$T_{min} = 0.649$, $T_{max} = 0.754$	$l = -13 \quad 11$
14673 measured reflections	
3746 independent reflections	

Refinement

Refinement on F^2	
Least-squares matrix: full	Hydrogen site location: mixed
$R[F^2 > 2\sigma(F^2)] = 0.040$	H atoms treated by a mixture of independent and constrained refinement
$wR(F^2) = 0.101$	$w = 1/[\sigma^2(F_o^2) + (0.0338P)^2 + 0.544P]$ where $P = (F_o^2 + 2F_c^2)/3$

S = 1.15	$(\Delta/\sigma)_{max} < 0.001$
3746 reflections	$\Delta\rho_{max}$ = 0.28 e Å^{-3}
362 parameters	$\Delta\rho_{min}$ = −0.19 e Å^{-3}
16 restraints	Extinction correction: SHELXL-2016/6 (Sheldrick 2016), $Fc^*=kFc[1+0.001xFc^2\lambda^3/\sin(2\theta)]^{-1/4}$
0 constraints	Extinction coefficient: 0.0084 (8)

Hydrogen-bond geometry (Å, °)

D—H···*A*	*D*—H	H···*A*	*D*···*A*	*D*—H···*A*
N1—H1*N*···O6	0.88 (2)	2.63 (2)	3.269 (2)	131 (2)
N1—H1*N*···O7*A*^{i}	0.88 (2)	2.21 (2)	2.955 (3)	142 (2)
N1—H1*M*···O1^{ii}	0.91 (2)	2.03 (2)	2.9398 (18)	177 (2)
N3—H3*N*···O8*A*^{iii}	0.89 (2)	2.24 (2)	3.119 (6)	170 (2)
N3—H3*N*···O8*B*^{iii}	0.89 (2)	2.27 (3)	3.15 (3)	169 (2)
N3—H3*M*···O2^{iv}	0.91 (1)	2.03 (2)	2.9380 (16)	172 (2)
O3—H3*O*···N4^{v}	0.88 (2)	1.74 (2)	2.6037 (16)	171 (2)
O6—H6*O*···N2^{vi}	0.89 (2)	1.74 (2)	2.6081 (17)	164 (2)
O8*A*—H8*O*···O4^{vii}	0.83 (2)	1.99 (2)	2.693 (11)	142 (3)
O8*A*—H8*O*···O9*A*	0.83 (2)	2.10 (3)	2.578 (7)	116 (3)
O9*A*—H9*O*···O2	0.84 (2)	1.98 (2)	2.818 (2)	170 (2)
O7*B*—H7*B*···O4*B*^{vii}	0.84	1.83	2.662 (13)	168
O9*B*—H9*B*···O5	0.84	2.63	3.055 (10)	113
Symmetry codes: (i) −*x*, −*y*+1, −*z*+1; (ii) −*x*, −*y*, −*z*+1; (iii) *x*, *y*−1, *z*; (iv) −*x*, −*y*, −*z*; (v) *x*−1, *y*, *z*−1; (vi) −*x*+1, −*y*+1, −*z*+2; (vii) −*x*, −*y*+1, −*z*.				

Table S6 - Crystal Structure of β Form.

Crystal data

$C_6H_8O_7 \cdot 2(C_6H_6N_2O)$	
$M_r = 436.38$	$D_x = 1.511$ Mg m^{-3}
Monoclinic, $P2_1/c$	
	Cu $K\alpha$ radiation, $\lambda = 1.54178$ Å
$a = 10.3854$ (4) Å	Cell parameters from 9843 reflections
$b = 21.0202$ (8) Å	$\theta = 3.3–72.2°$
$c = 17.6219$ (7) Å	$\mu = 1.06$ mm^{-1}
$\beta = 94.0777$ (16)°	$T = 173$ K
$V = 3837.2$ (3) Å^3	Block, colourless
$Z = 8$	0.36 × 0.15 × 0.11 mm
$F(000) = 1824$	

Bruker D8 Venture Photon diffractometer	6685 reflections with $I > 2\sigma(I)$
Radiation source: IμS Cu	$R_{int} = 0.047$
	$\theta_{max} = 72.2°$, $\theta_{min} = 3.3°$
φ and ω scans	$h = -12 \quad 12$
Absorption correction: multi-scan *SADABS* 2016/2: Krause, L., Herbst-Irmer, R., Sheldrick G.M. & Stalke D., J. Appl. Cryst. 48 (2015) 3-10	$k = -25 \quad 25$
$T_{min} = 0.651$, $T_{max} = 0.754$	$l = -21 \quad 21$
40494 measured reflections	
7534 independent reflections	

Refinement

Refinement on F^2	
Least-squares matrix: full	Hydrogen site location: mixed
$R[F^2 > 2\sigma(F^2)] = 0.050$	H atoms treated by a mixture of independent and constrained refinement
$wR(F^2) = 0.114$	$w = 1/[\sigma^2(F_o^2) + (0.0269P)^2 + 3.4024P]$ where $P = (F_o^2 + 2F_c^2)/3$
$S = 1.13$	$(\Delta/\sigma)_{max} < 0.001$
7534 reflections	$\Delta\rho_{max} = 0.43$ e Å^{-3}
607 parameters	$\Delta\rho_{min} = -0.25$ e Å^{-3}
16 restraints	Extinction correction: none
0 constraints	

Hydrogen-bond geometry (Å, °)

D—H···*A*	*D*—H	H···*A*	*D*···*A*	*D*—H···*A*
N1—H1*N*···O2^{i}	0.90 (2)	2.04 (2)	2.942 (2)	179 (3)
N1—H1*M*···O10^{ii}	0.89 (2)	2.35 (2)	3.118 (3)	145 (3)
O5—H5*O*···N4^{iii}	0.87 (2)	1.78 (2)	2.624 (2)	164 (3)
O7—H7*O*···N6^{i}	0.88 (2)	1.73 (2)	2.609 (2)	171 (3)
O10—H10*O*···O11	0.84 (2)	1.93 (2)	2.5337 (19)	127 (2)
O10—H10*O*···O12	0.84 (2)	2.16 (2)	2.768 (2)	129 (2)
O11—H11*O*···O4^{iv}	0.87 (2)	1.89 (2)	2.7430 (19)	167 (2)
N3—H3*N*···O1^{i}	0.91 (2)	2.01 (2)	2.912 (2)	176 (2)
N3—H3*M*···O17	0.90 (2)	2.19 (2)	3.014 (2)	153 (2)
N5—H5*N*···O4^{iv}	0.91 (2)	2.09 (2)	2.997 (2)	174 (2)
N5—H5*M*···O16	0.91 (2)	2.15 (2)	3.052 (2)	170 (2)
N7—H7*N*···O3^{v}	0.90 (2)	2.05 (2)	2.946 (2)	174 (2)
N7—H7*M*···O9	0.89 (2)	2.11 (2)	2.986 (2)	170 (2)
O13—H13*O*···N8^{vi}	0.85 (2)	1.77 (2)	2.610 (2)	171 (3)
O15—H15*O*···N2^{vii}	0.85 (2)	1.80 (2)	2.619 (2)	162 (3)
O16—H16*O*···O8	0.85 (2)	2.02 (2)	2.737 (2)	142 (2)
O16—H16*O*···O18	0.85 (2)	2.04 (2)	2.550 (2)	118 (2)
O18—H18*O*···O2^{viii}	0.88 (2)	1.91 (2)	2.775 (2)	169 (2)

Symmetry codes: (i) −*x*, −*y*+1, −*z*+1; (ii) *x*, −*y*+1/2, *z*+1/2; (iii) −*x*+1, −*y*+1, −*z*; (iv) −*x*+1, *y*+1/2, −*z*+1/2; (v) −*x*+1, *y*−1/2, −*z*+1/2; (vi) *x*, −*y*+1/2, *z*−1/2; (vii) *x*−1, *y*, *z*; (viii) −*x*, *y*−1/2, −*z*+1/2.

Table S7 - Crystal Structure of γ Form

Crystal data

$C_6H_8O_7 \cdot 2(C_6H_6N_2O)$	
$M_r = 436.38$	$D_x = 1.502$ Mg m^{-3}
Monoclinic, *Cc*	
	Cu *K*α radiation, λ = 1.54178 Å
a = 31.4521 (12) Å	Cell parameters from 7302 reflections
b = 5.3196 (2) Å	θ = 2.9–72.2°
c = 11.7729 (5) Å	μ = 1.05 mm^{-1}
β = 101.4741 (19)°	*T* = 173 K
V = 1930.39 (13) Å^3	Needle, colourless
Z = 4	0.46 × 0.11 × 0.05 mm
F(000) = 912	

Data collection

Bruker D8 Venture Photon diffractometer	3386 reflections with $I > 2\sigma(I)$
Radiation source: IμS Cu	$R_{int} = 0.046$
	$\theta_{max} = 72.2°$, $\theta_{min} = 2.9°$
φ and ω scans	$h = -38 \quad 38$
Absorption correction: multi-scan SADABS 2016/2: Krause, L., Herbst-Irmer, R., Sheldrick G.M. & Stalke D., J. Appl. Cryst. 48 (2015) 3-10	$k = -6 \quad 6$
$T_{min} = 0.627$, $T_{max} = 0.754$	$l = -14 \quad 14$
9836 measured reflections	
3610 independent reflections	

Refinement

Refinement on F^2	Hydrogen site location: mixed
Least-squares matrix: full	H atoms treated by a mixture of independent and constrained refinement
$R[F^2 > 2\sigma(F^2)] = 0.045$	$w = 1/[\sigma^2(F_o^2) + (0.0689P)^2 + 1.4786P]$ where $P = (F_o^2 + 2F_c^2)/3$
$wR(F^2) = 0.120$	$(\Delta/\sigma)_{max} < 0.001$
S = 1.05	$\Delta\rho_{max} = 0.44$ e Å^{-3}
3610 reflections	$\Delta\rho_{min} = -0.27$ e Å^{-3}
305 parameters	Extinction correction: none
12 restraints	
0 constraints	Absolute structure: Refined as an inversion

	twin.
	Absolute structure parameter: 0.4 (3)

Refined as a 2-component inversion twin.

Hydrogen-bond geometry (Å, °)

D—H···*A*	*D*—H	H···*A*	*D*···*A*	*D*—H···*A*
N1—H1*M*···O3^{i}	0.87 (3)	2.05 (3)	2.893 (5)	164 (5)
N1—H1*N*···O2^{ii}	0.92 (3)	1.97 (3)	2.875 (5)	170 (5)
C3—H3···O2^{iii}	0.95	2.52	3.192 (5)	128
C6—H6···O3^{i}	0.95	2.42	3.347 (6)	167
N3—H3*N*···O1^{iv}	0.88 (3)	2.03 (3)	2.901 (4)	174 (5)
N3—H3*M*···O5^{v}	0.90 (3)	1.98 (3)	2.860 (4)	164 (5)
C9—H9···O5^{v}	0.95	2.39	3.310 (5)	163
C10—H10···O7^{vi}	0.95	2.56	3.391 (5)	146
C10—H10···O8^{v}	0.95	2.52	3.218 (5)	130
C11—H11···O1^{vii}	0.95	2.60	3.181 (5)	120
C12—H12···O1^{vii}	0.95	2.59	3.170 (5)	120
O4—H4*O*···N2	0.87 (2)	1.80 (2)	2.608 (5)	153 (5)
O6—H6*O*···N4	0.85 (2)	1.71 (2)	2.560 (4)	173 (6)
O7—H7*O*···O6^{viii}	0.83 (3)	1.89 (4)	2.600 (4)	143 (5)
O7—H7*O*···O9^{viii}	0.83 (3)	2.52 (5)	3.081 (4)	126 (5)
C16—H16*A*···O8^{ix}	0.99	2.53	3.470 (5)	159

Table S8 - Crystal Structure of Salt Form.

Crystal data

$C_6H_7O_7 \cdot C_6H_6N_2O \cdot C_6H_7N_2O$	$F(000) = 456$
$M_r = 436.38$	
Triclinic, P	$D_x = 1.541$ Mg m^{-3}
$a = 9.5658$ (3) Å	Cu $K\alpha$ radiation, $\lambda = 1.54178$ Å
$b = 10.6257$ (4) Å	Cell parameters from 9855 reflections
$c = 11.3057$ (4) Å	$\theta = 4.5$–$72.4°$
$\alpha = 111.3323$ (10)°	$\mu = 1.08$ mm^{-1}
$\beta = 102.8329$ (11)°	$T = 173$ K
$\gamma = 108.2681$ (10)°	Block, colourless
$V = 940.21$ (6) Å^3	0.46 × 0.20 × 0.17 mm
$Z = 2$	

Data collection

Bruker D8 Venture Photon diffractometer	3473 reflections with $I > 2\sigma(I)$
Radiation source: IμS Cu	$R_{int} = 0.035$
	$\theta_{max} = 72.4°$, $\theta_{min} = 4.5°$
φ and ω scans	$h = -11 \quad 11$
Absorption correction: multi-scan *SADABS* 2016/2: Krause, L., Herbst-Irmer, R., Sheldrick G.M. & Stalke D., J. Appl. Cryst. 48 (2015) 3-10	$k = -13 \quad 12$
$T_{min} = 0.603$, $T_{max} = 0.754$	$l = -13 \quad 13$
18147 measured reflections	
3691 independent reflections	

Refinement

Refinement on F^2	
Least-squares matrix: full	Hydrogen site location: mixed
$R[F^2 > 2\sigma(F^2)] = 0.035$	H atoms treated by a mixture of independent and constrained refinement
$wR(F^2) = 0.093$	$w = 1/[\sigma^2(F_o^2) + (0.0491P)^2 + 0.3315P]$ where $P = (F_o^2 + 2F_c^2)/3$
$S = 1.05$	$(\Delta/\sigma)_{max} < 0.001$
3691 reflections	$\Delta\rho_{max} = 0.32$ e Å^{-3}
329 parameters	$\Delta\rho_{min} = -0.26$ e Å^{-3}
10 restraints	Extinction correction: none
0 constraints	

Hydrogen-bond geometry (Å, °)

D—H···*A*	*D*—H	H···*A*	*D*···*A*	*D*—H···*A*
N1—H1*N*···O5^{i}	0.90 (1)	1.99 (2)	2.8778 (15)	169 (2)
N1—H1*M*···O2^{ii}	0.91 (1)	1.95 (2)	2.853 (6)	176 (2)
N1—H1*M*···O2*B*^{ii}	0.91 (1)	1.99 (2)	2.878 (12)	165 (2)
N2—H2*N*···O7	0.97 (1)	1.64 (1)	2.5840 (13)	165 (2)
N2—H2*N*···O9	0.97 (1)	2.57 (2)	3.1587 (13)	119 (1)
C3—H3···O5^{i}	0.95	2.39	3.3125 (15)	163
C4—H4···O9	0.95	2.46	3.1085 (15)	126
C6—H6···O8^{iii}	0.95	2.58	3.2629 (15)	130
N3—H3*N*···O1^{ii}	0.91 (2)	2.00 (2)	2.908 (3)	174 (3)
N3—H3*M*···O9^{i}	0.88 (2)	2.25 (2)	3.103 (3)	162 (2)
N3*B*—H3*O*···O1^{ii}	0.92 (2)	2.01 (2)	2.919 (7)	169 (5)
C9—H9···O3^{iv}	0.95	2.42	3.3208 (15)	159
C10—H10···O5	0.95	2.51	3.1212 (15)	123
C11—H11···O7^{iii}	0.95	2.32	3.2535 (14)	167
O4—H4*O*···O8^{v}	0.89 (1)	1.64 (1)	2.5360 (12)	175 (2)
O6—H6*O*···N4	0.94 (1)	1.66 (1)	2.5991 (13)	176 (2)
O9—H9*O*···O3	0.83 (1)	2.16 (2)	2.7901 (12)	132 (1)
O9—H9*O*···O3^{vi}	0.83 (1)	2.30 (2)	2.9370 (12)	133 (1)
C14—H14*A*···O2*B*^{vii}	0.99	2.60	3.506 (11)	153
C14—H14*B*···O8^{v}	0.99	2.66	3.2997 (13)	123

Crystal Packing Images

***α* Form**

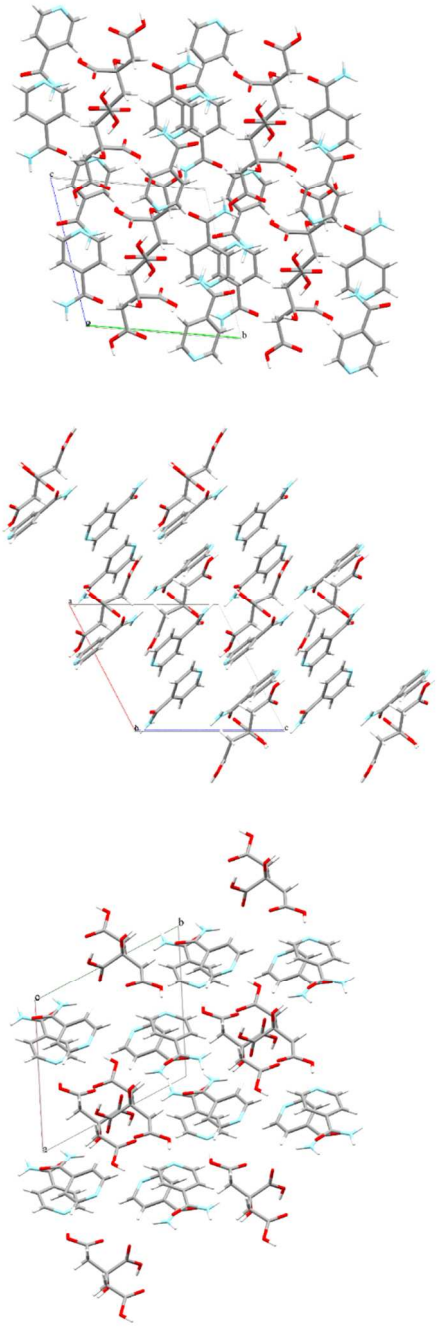

Figure S5 - α Form Down a-axis (top). Down b-axis (middle). Down c-axis (bottom).

***β* Form**

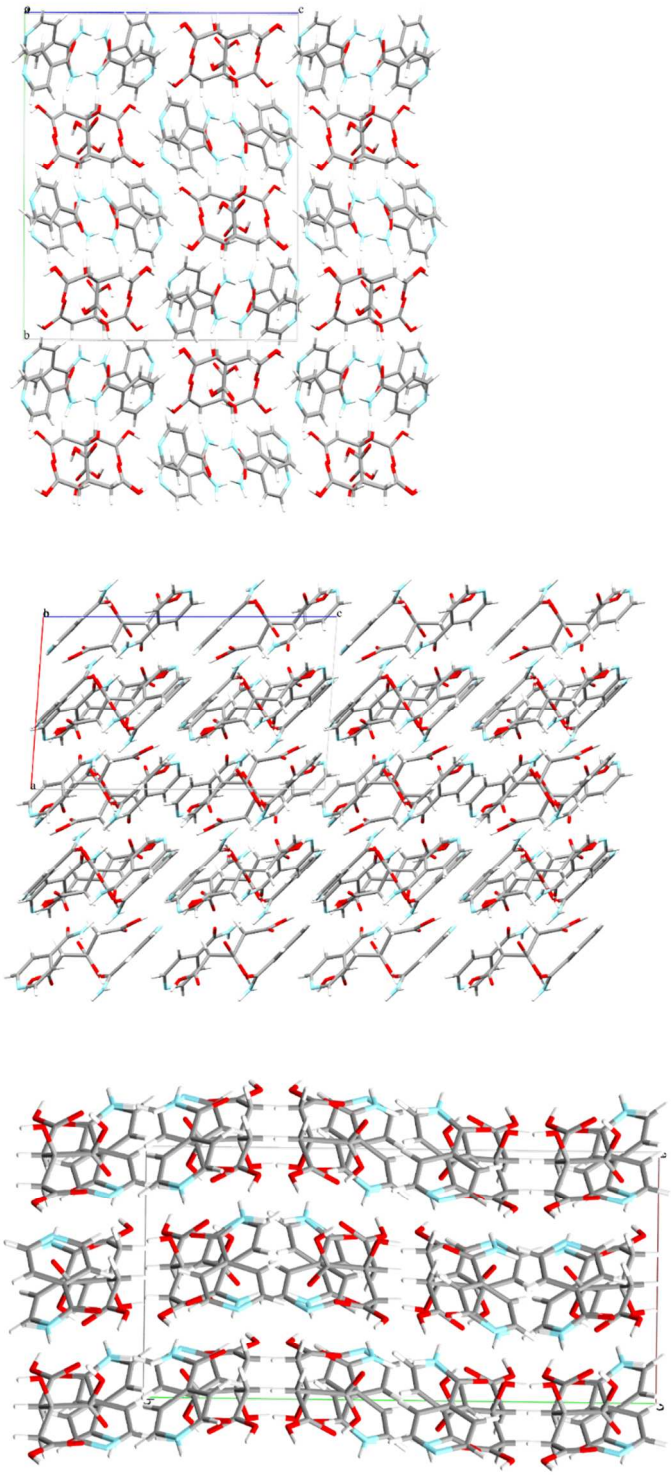

Figure S6 - β Form Down a-axis (top). Down b-axis (middle). Down c-axis (bottom).

***γ* Form**

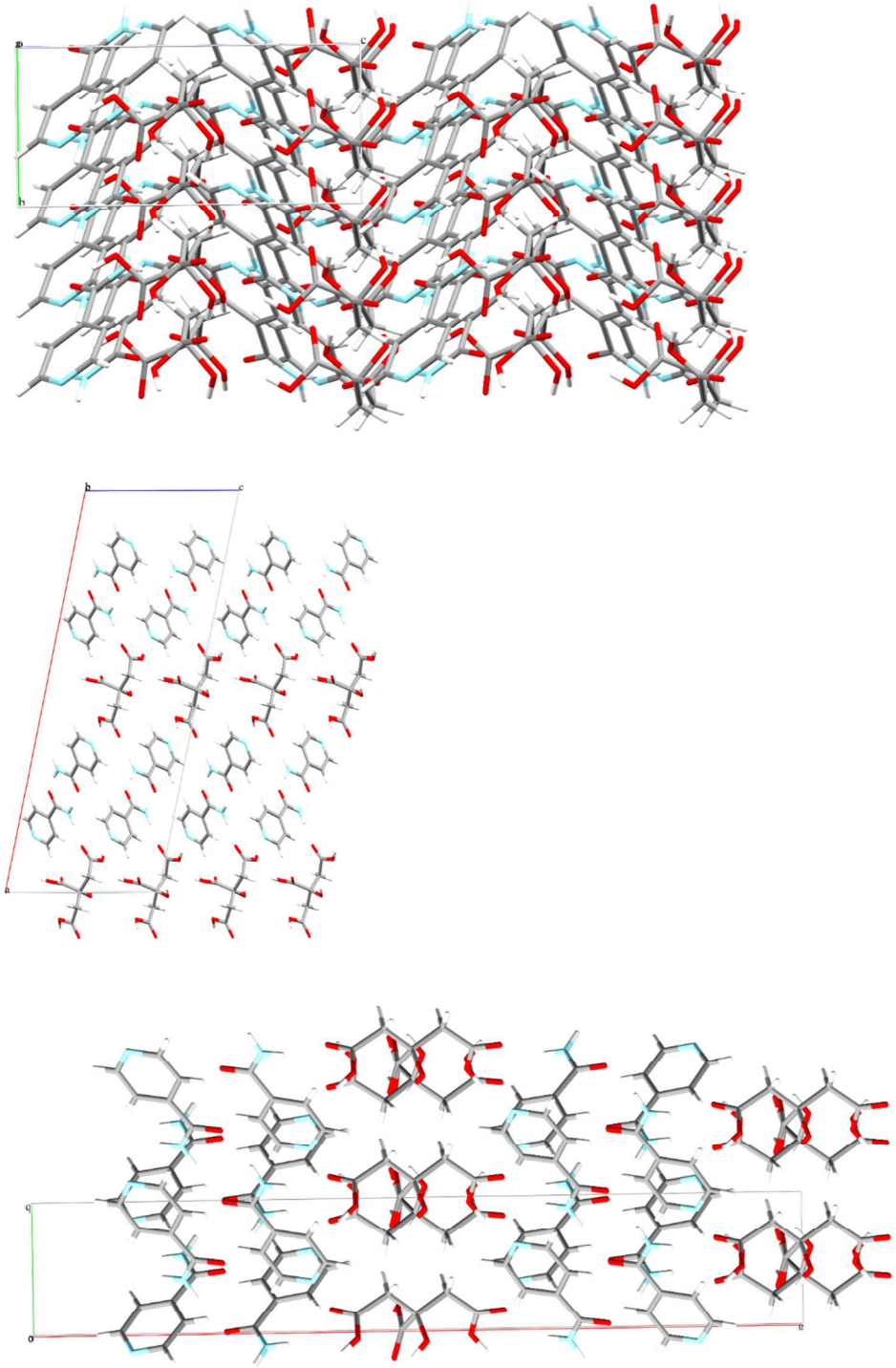

Figure S7 - γ Form Down a-axis (top). Down b-axis (middle). Down c-axis (bottom).

Salt Form

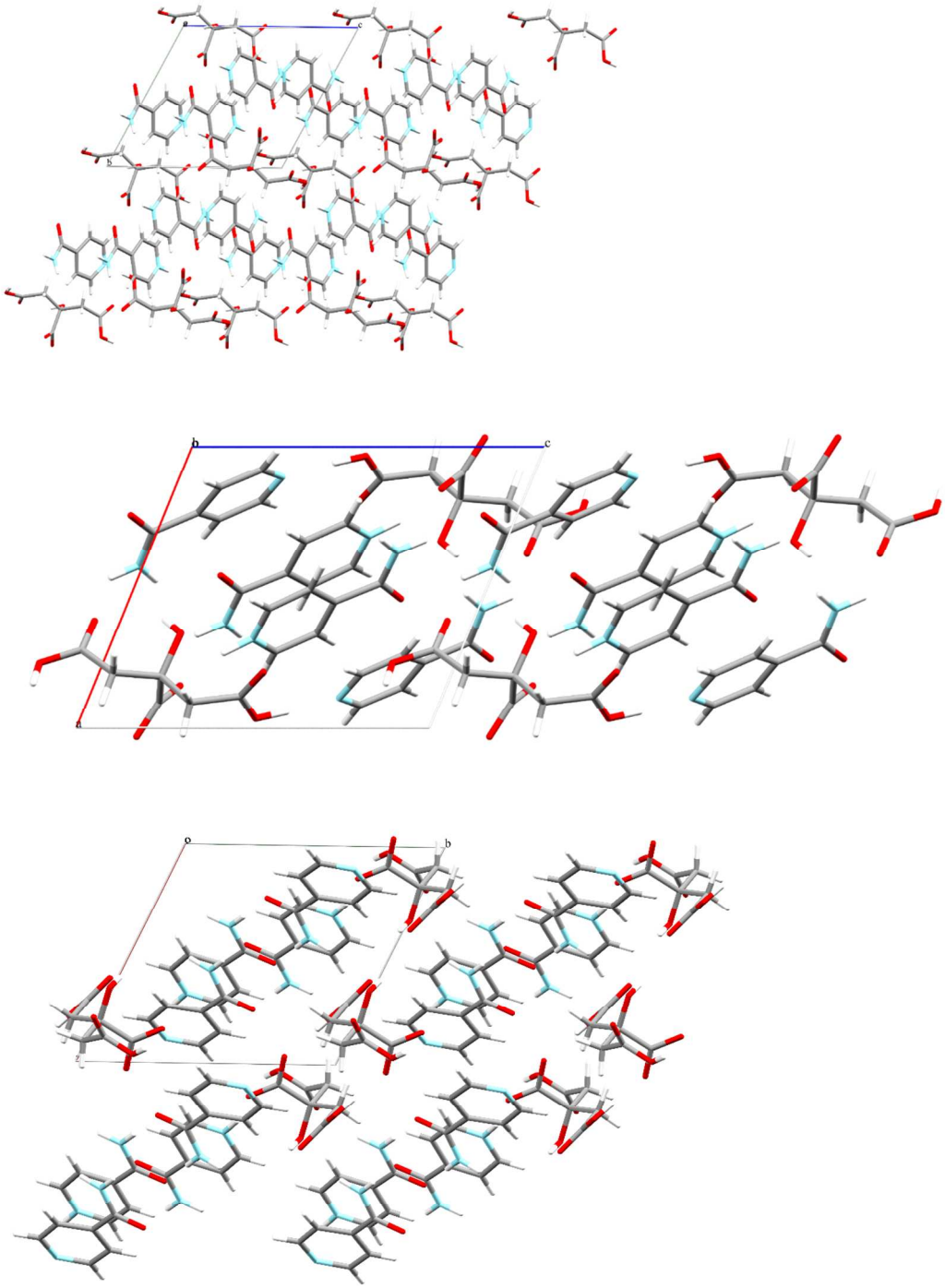

Figure S8 - Salt Form Down a-axis (top). Down b-axis (middle). Down c-axis (bottom).

3. Supporting characterisation

Differential Scanning Calorimetry

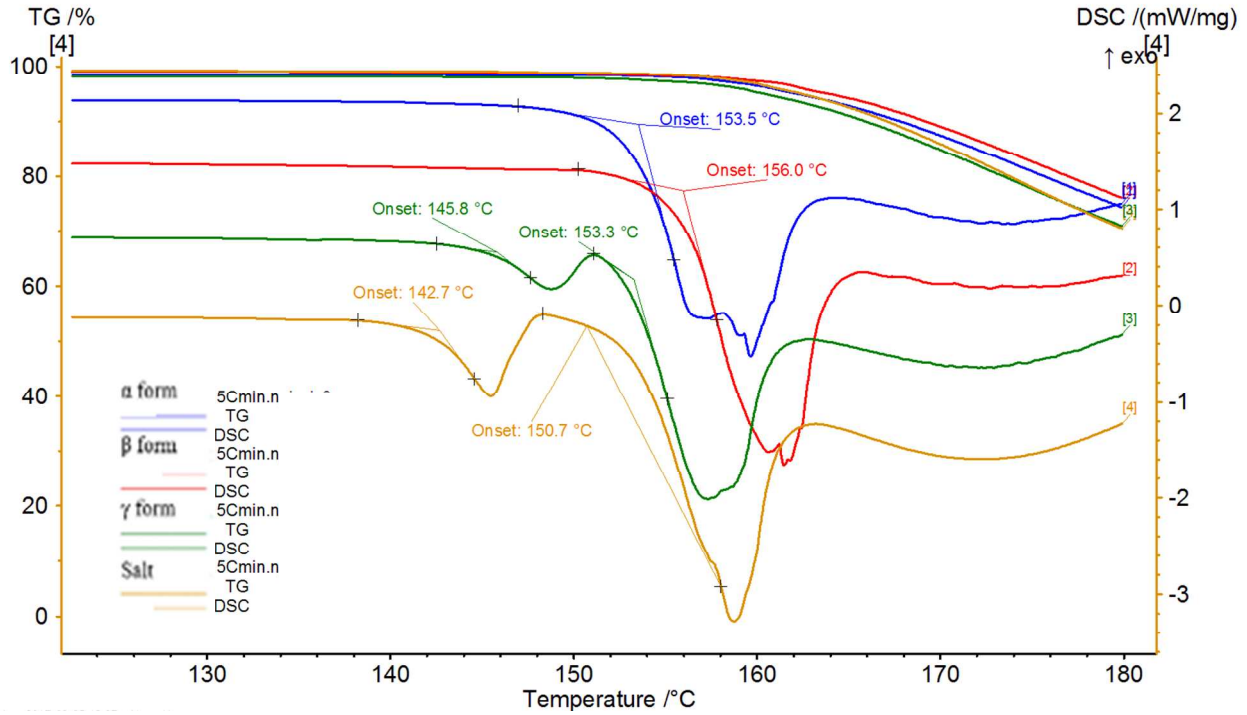

Figure S9 - DSC and TGA Ramped at 5°C/min

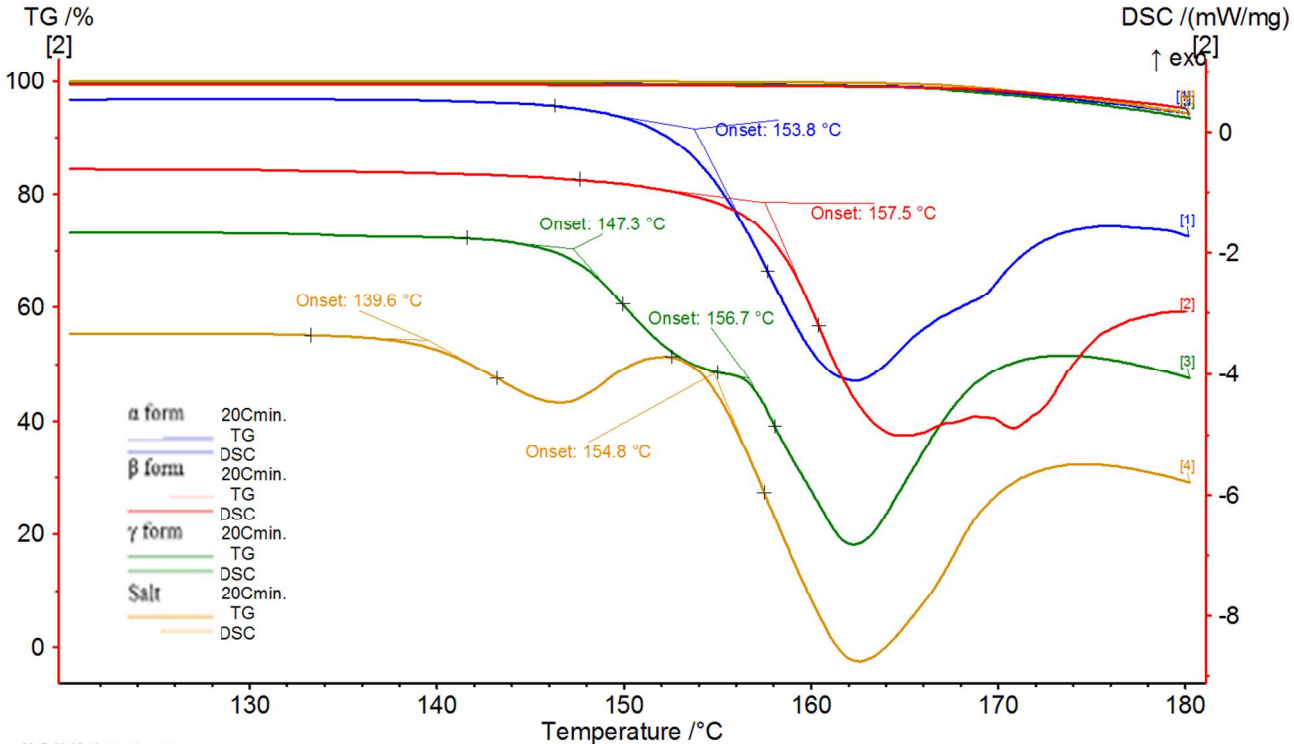

Figure S10 - DSC and TGA Ramped at 20°C/min.

Hot Stage Microscopy (HSM) Images

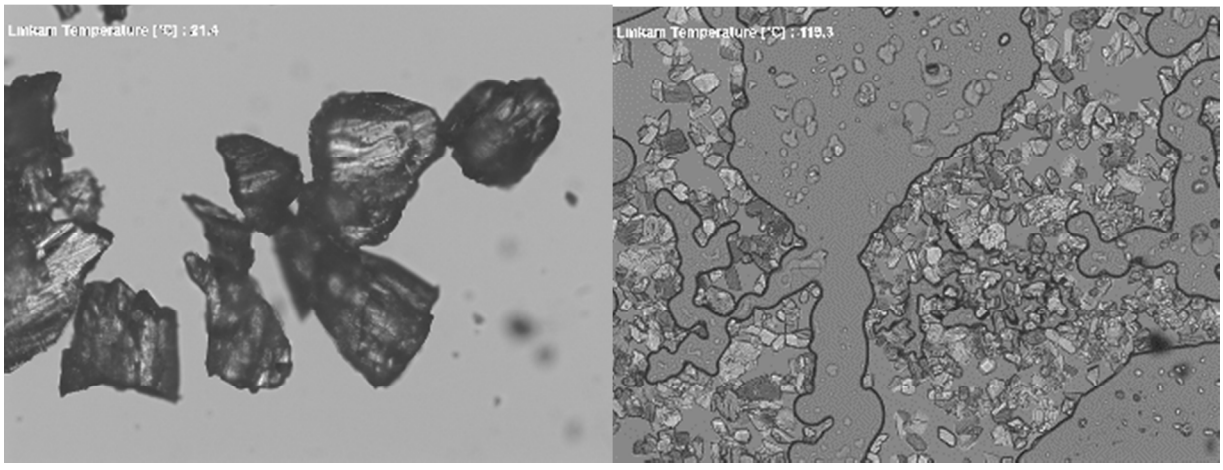

Figure S11 – HSM of α form.

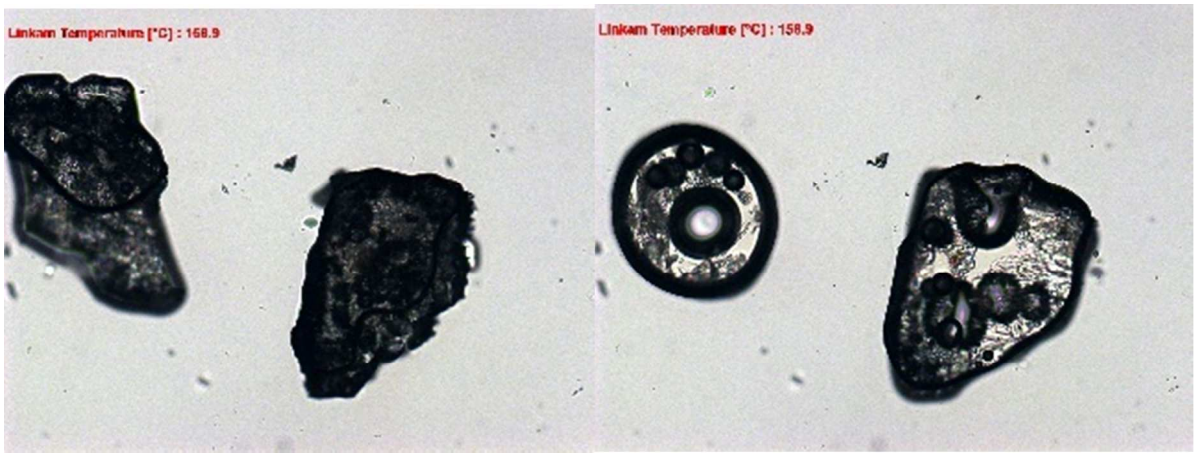

Figure S12 – HSM of β form.

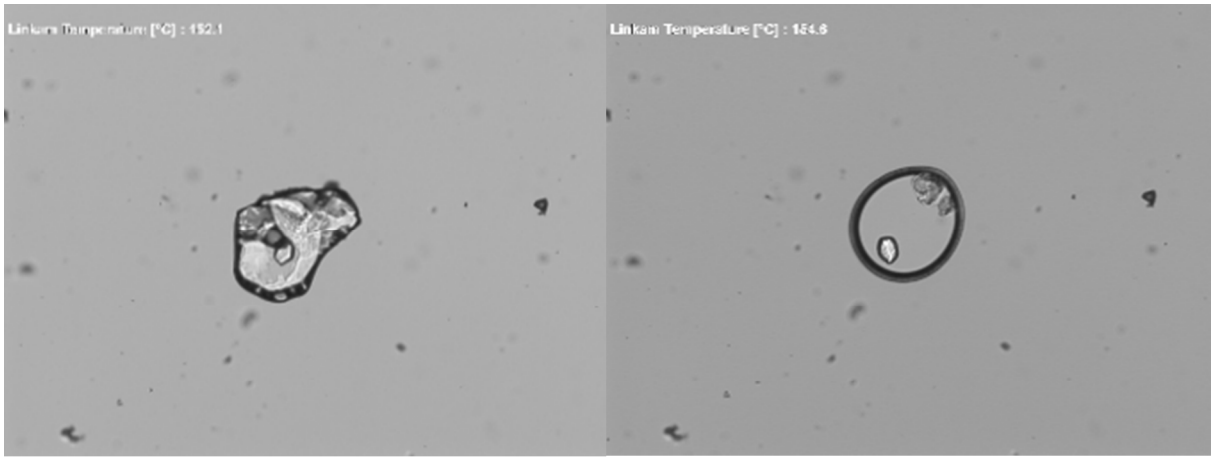

Figure S13 – HSM of γ form.

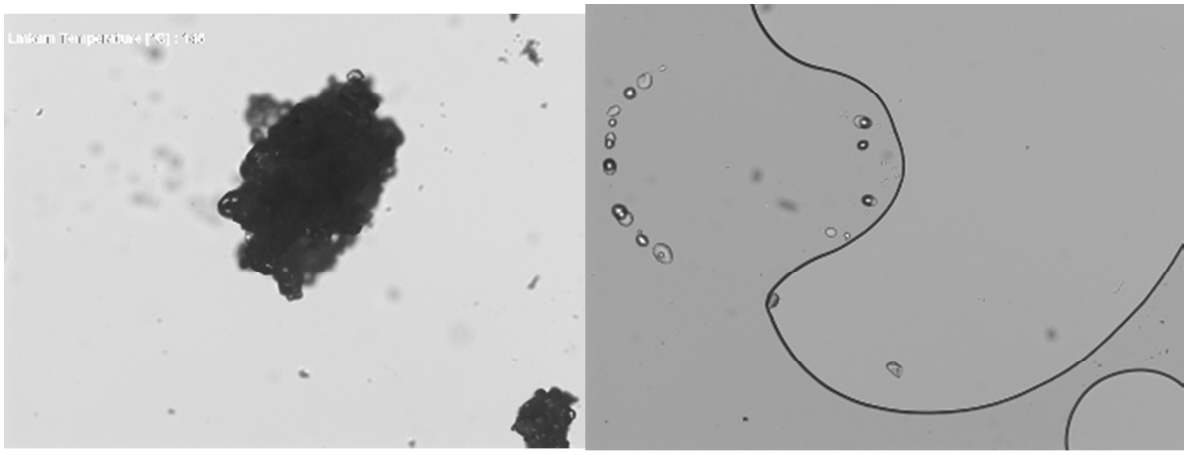

Figure S14 – HSM of salt form.

Solubility and Spectroscopy Studies

The relative solubility of each form was gauged by weight, 0.1g employed and placed in vial, and subsequent addition of selected solvent was undertaken. Solvents used pure water, 50:50 water: ethanol and pure ethanol. Aliquots dispensing was undertaken using the autopipetting Zinsser LISSY in 100µl increments, mixing after each addition, until dissolved.

Table S9 – Solubility Estimates.

Sample	Citric Acid	Isonicotinamide	*α*	*β*	*γ*	Salt
Solubility in Water (mg/l)	802.9	191.7	35.9	46.1	45.5	52.7
Solubility in 50:50 EtOH: H2O (mg/l)	657.9	104.7	23.7	18.5	32.2	22.3
Solubility in EtOH (mg/l)	223.5	166.87	25.6	11.4	6.5	8.3

FT-IR

FT-IR spectra were acquired using a Perkin-Elmer Spectrum 100 FT-IR Spectrometer. The background was measured before each sample was measured with 16 acquisitions.

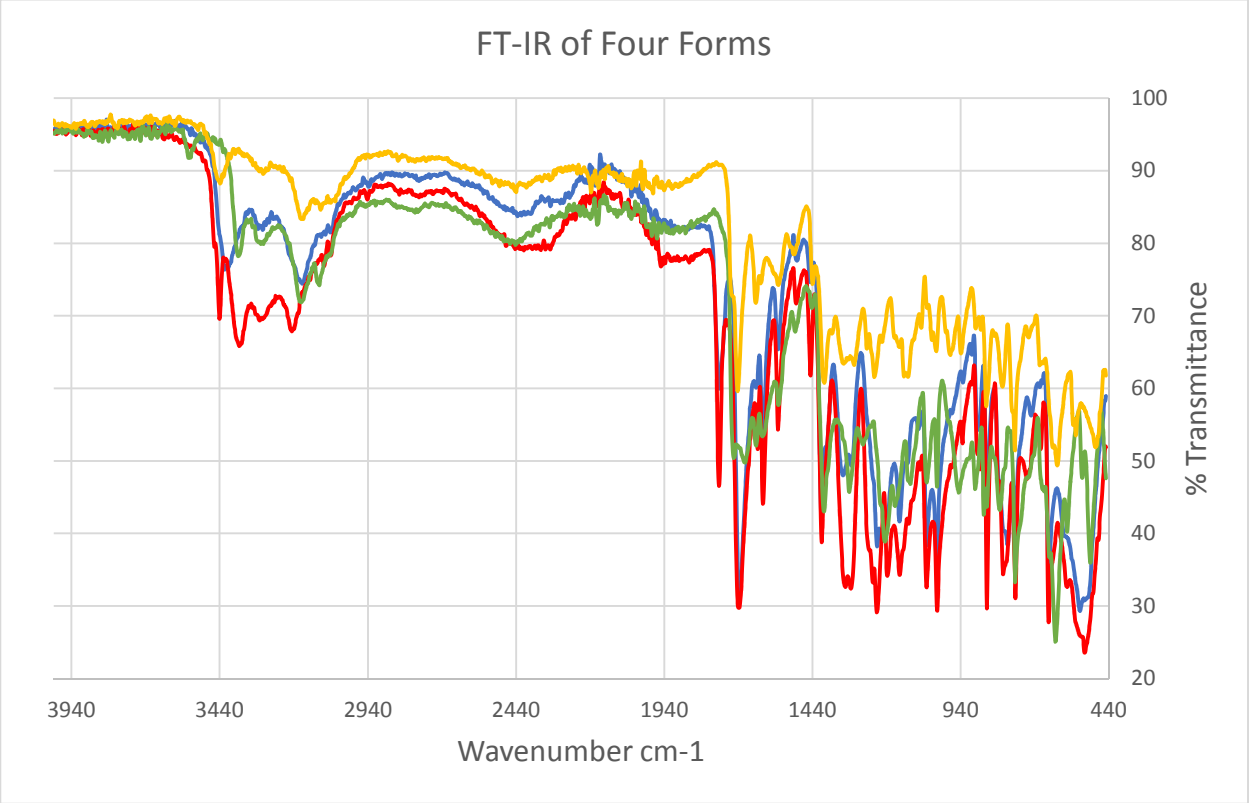

Figure S15 - FT-IR of four forms overlaid: α (blue), β (red), γ (green), salt (orange).

Raman

Raman spectra of each sample were measured on a Bruker Senterra using the 785nm laser operating at 100mW with an acquisition rate of 8 or 16 scans within a 2 seconds period.

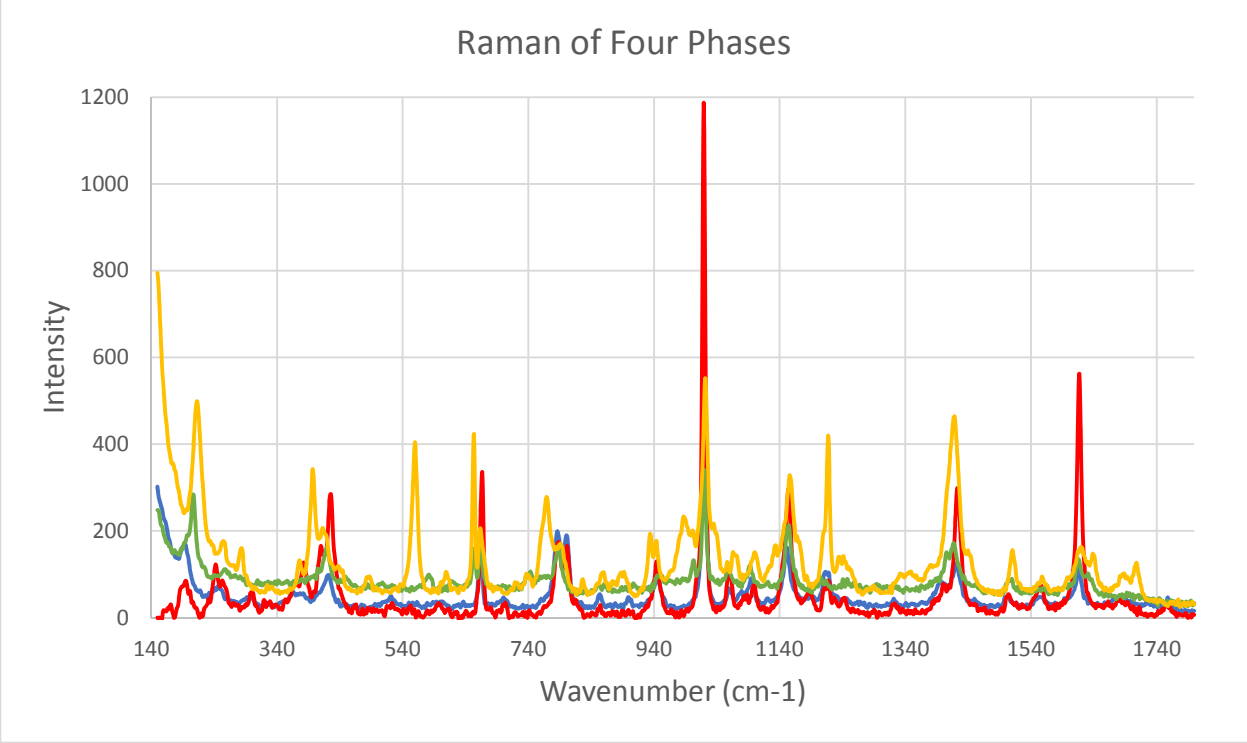

Figure S16 - Raman of α (blue), β (red), γ (green) and the salt (orange) overlaid.

4 Supporting Narrative: Hydrogen Bond Network from pairwise and beyond….

This section is included to communicate the base level analysis undertaken on the four forms isolated with regards pairwise motifs (synthons), and the notion of complex or ionic form in the context of crystal growth units. All which employs supporting information from sections 1-3.

They key view of these motifs is found within the growth units theme within the paper. See figures below I to VII, it is important to appreciate that these units are dependant on how the supramolecular construct is employed and a number of possible combinations for a specific form may be generated.

homo-molecular motifs

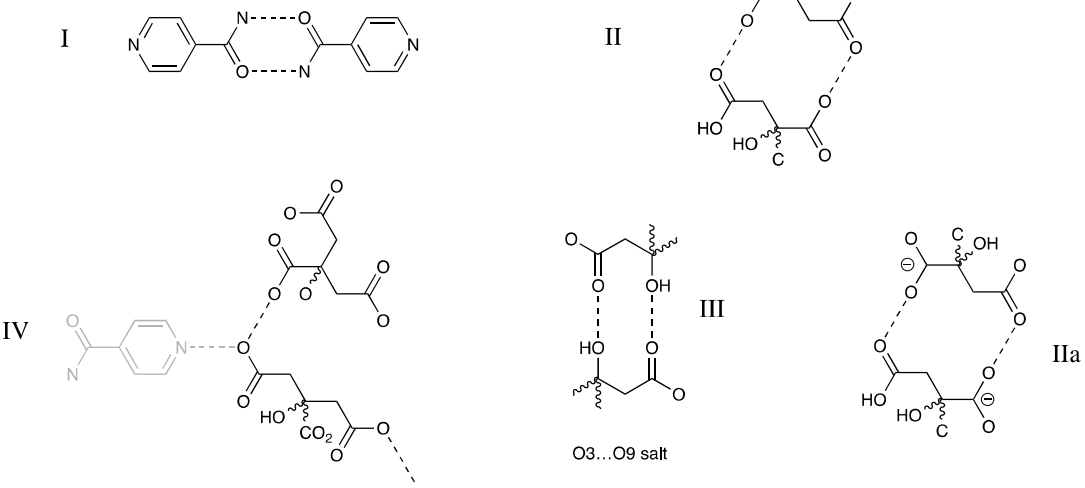

hetero-molecular motifs

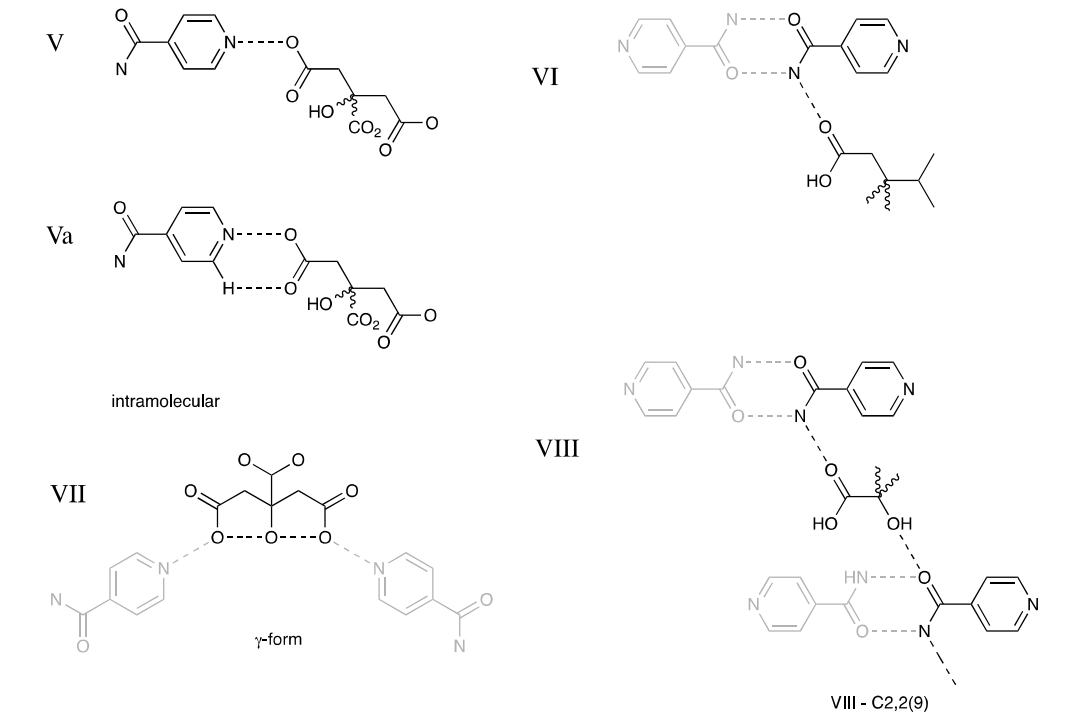

With regards to the link of these motifs and the crystallisation, the reader is directed to growth units, as these set specific boundaries that are employed within the narrative in the paper. In that the shortest atom connectivity is aligned to graphs sets and is manifested in the growth unit for layer assembly. This approach reflects development of the asymmetric unit within a growth picture for the system being examined. *See below top LHS alpha, bottom LHS beta, top RHS gamma, bottom RHS salt*.

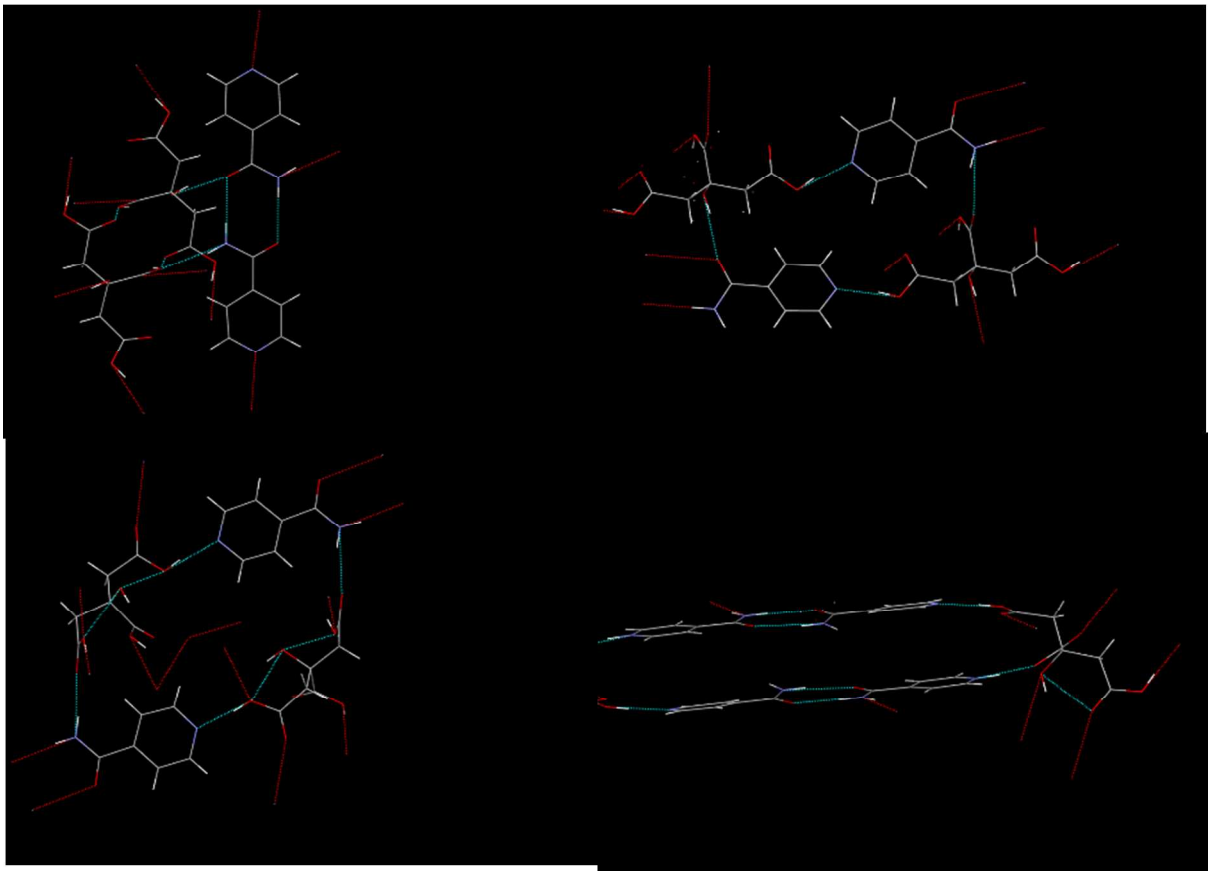

In this way the pairwise assemblies are linked to the notion of growth as a layer by layer process, which is based within the E_{att} approach to morphology and intermolecular contacts.

One allied issue is the view of a hydrogen bond within the context of the position, contact and localisation of the hydrogen along such an intermolecular interaction; which may be expressed either as an ionic framework or as a polar framework. The situation is identifiable through secondary evidence of: bond lengths, torsions and primary evidence: charge density maps between acid and basic sites. In this regard, evidence from the generation of the difference (F_o-F_c map) for the assigned salt, whereby the removal of the proton from the 'protonated' ionic form, the resulting map clearly demonstrates unambiguously the localisation of the proton position to the pyridine nitrogen and, notably, no significant electron destiny is associated with the oxygen (O7) of the 'citrate'. The peak is 0.73 eA^{-3} is consistent with localisation of the proton at this position and its inclusion at full occupancy in the model significantly reduces the *R*-factor.

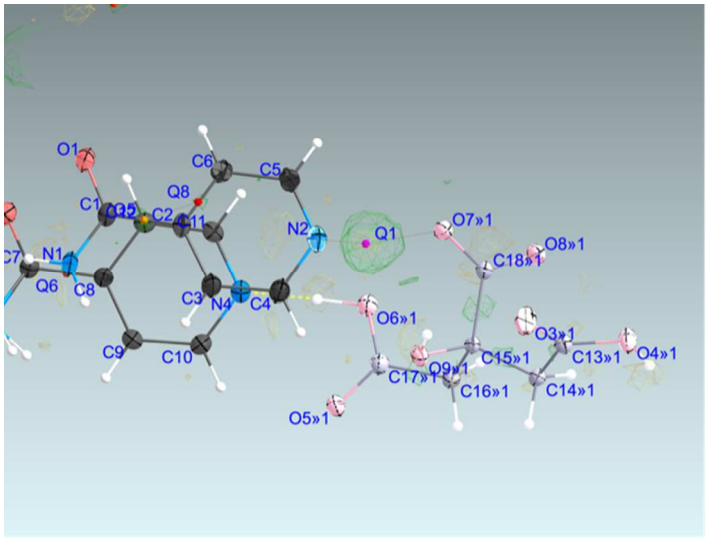

This view is also backed up by the vibrational spectroscopy, particularly Raman spectroscopy, which also provides differentiation between each phase and provides some insight into the structural role of the coformers. Raman spectra of the products are shown below.

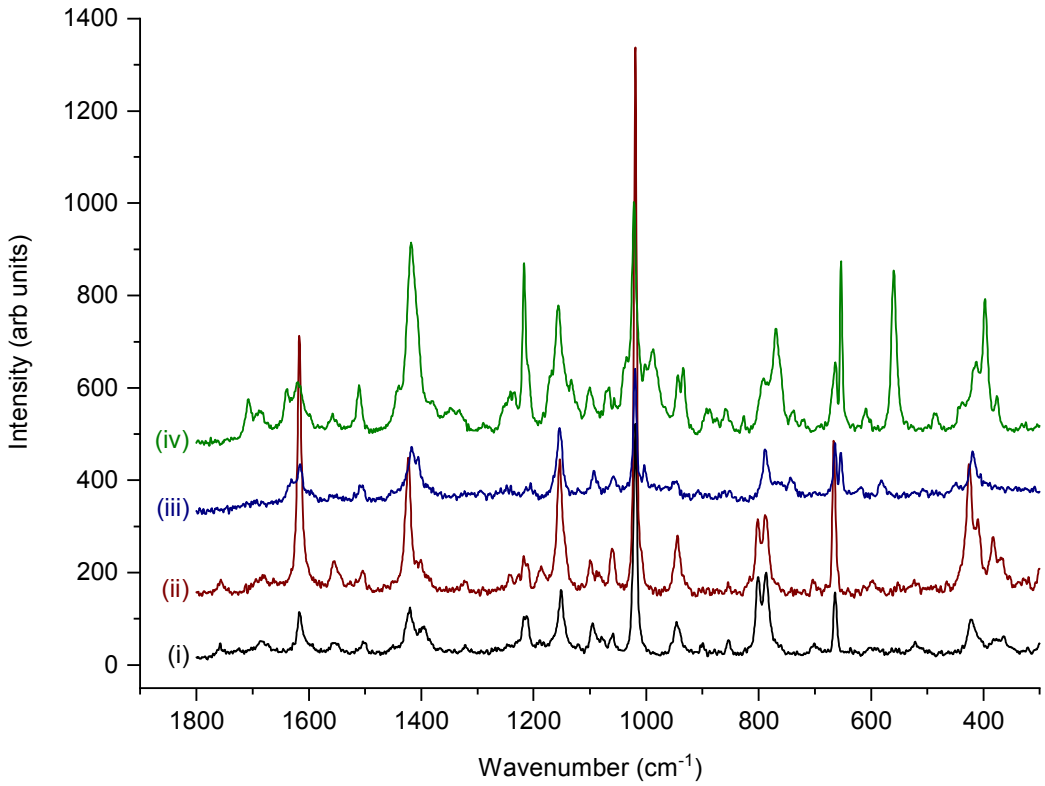

Note: Raman spectra of the four forms with 785 nm excitation: (i) *α*-form (black), *β*-form (red), *γ*-form (blue), salt-form (green).

It is interesting to note, that the spectra of the *α*- and *β*-form are similar and consistent with the close relation between polytypes. The salt and *γ*-forms can be differentiated from these, and from each other, through different spectral envelopes in the following regions: 1800-1630 cm^{-1}, associated with C=O stretching modes of the citric acid; 1100-1040 cm^{-1} and *ca.* 940 cm^{-1}, consistent with C-O stretching modes of CA [L.C. Bichara, et al Adv. Phys. Chem., 2011, 2011, ID 347072, doi:10.1155/2011/347072]. The spectrum of the salt features a strong and definitive band at 560 cm^{-1}, tentatively assigned to N-H bending modes of the protonated IN [D. Cook, Can J. Chem, 1961, 39, 2009., A.A. Samoilenko, et al. J. Struct Chem 17(4) 546-552, (1977)]. In contrast to CA, the IN components in the spectrum remain largely unchanged between phases. In particular, the position intense band associated with the ring breathing mode of pyridine of IN at *ca.* 1020 cm^{-1} is essentially constant for the co-crystal forms (1019 cm^{-1} for *α*- and *β*-forms, 1020 cm^{-1} for the *γ*-form) and shifts marginally for the salt (1022 cm^{-1}) and this presumably originates from its common role in the structures with the hydrogen-bonded amide-amide dimer [S.A. Kulkarni, et al ChemCommun 2012, 48, 4983-4985]. Similarly, the amide scissoring mode of IN stays remarkably constant at 1617 cm^{-1} across the forms as does the ring stretching and deformation mode at 1154 and 667 cm^{-1} respectively [M. Bakiler et al. J. Mol. Struct., 2007, 826, 6–16]. Clearly, the vibrational spectroscopic data points to a relatively similar structural role for IN in the phases, with the predominant variations occurring with the CA coformer

This pre work was employed to mitigate the use of complex/co crystal and salt form employed in the paper. It was placed in the supplementary information in order to improve the readability of the paper with a crystallisation perspective. Consequently, the critical secondary structural information is as follows:

Alpha Form

Number	Object1	Object2	Object3	Object4	Torsion
1	O9A	C15A	C18A	O8A	-1.6(5)
2	O9A	C15A	C14	C13	-63.2(3)
3	O9A	C15A	C16	C17	65.8(3)
4	C15A	C14	C13	O3	158.9(2)
5	C15A	C16	C17	O6	-140.9(2)

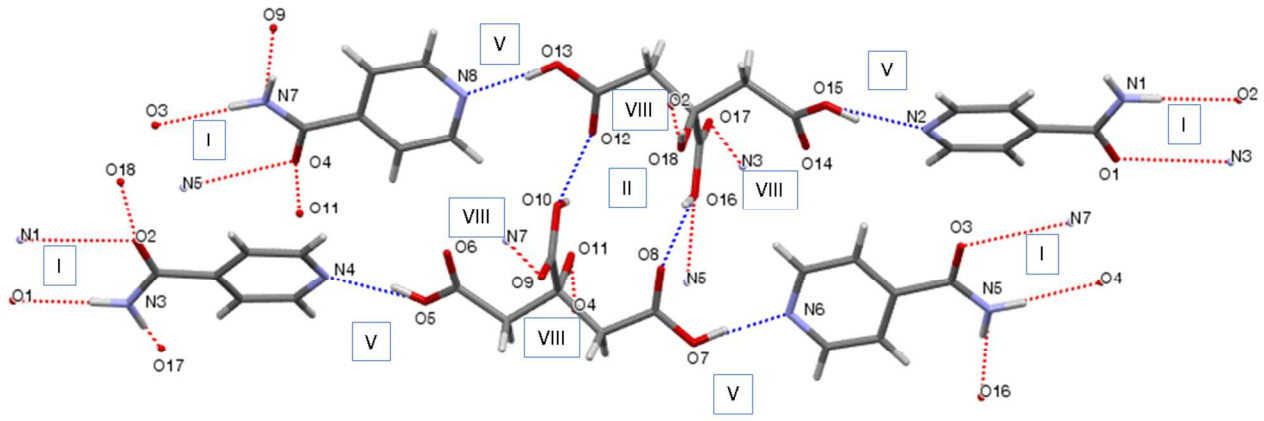

Beta Form

Number	Object1	Object2	Object3	Object4	Torsion
1	O11	C27	C30	O10	1.9(2)
2	O11	C27	C26	C25	-66.2(2)
3	O11	C27	C28	C29	60.9(2)
4	C27	C26	C25	O5	139.7(2)
5	C27	C28	C29	O7	-155.2(2)
6	O18	C33	C36	O16	-2.6(2)
7	O18	C33	C32	C31	-62.5(2)
8	O18	C33	C34	C35	66.9(2)
9	C33	C32	C31	O13	150.8(2)
10	C33	C34	C35	O15	-136.5(2)

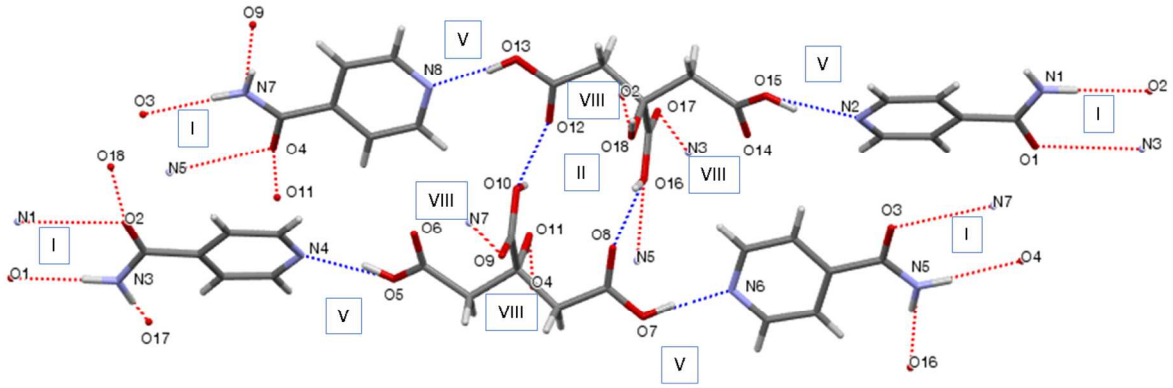

Gamma Form

Number	Object1	Object2	Object3	Object4	Torsion
1	O9	C15	C18	O7	167.1(3)
2	O9	C15	C14	C13	-46.6(4)
3	O9	C15	C16	C17	65.8(4)
4	C15	C14	C13	O4	-49.3(5)
5	C15	C16	C17	O6	-69.9(4)

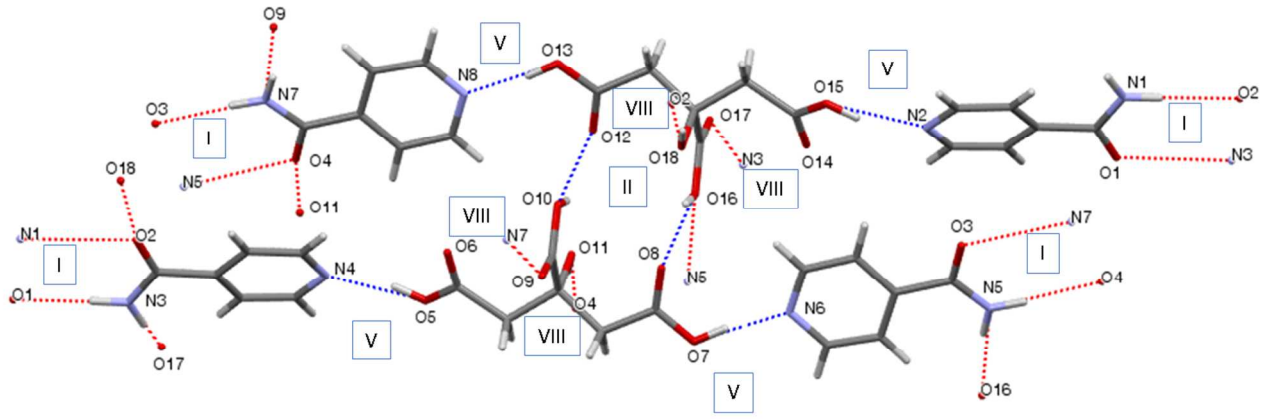

Salt Form

Number	Object1	Object2	Object3	Object4	Torsion
1	O9	C15	C18	O7	-9.5(2)
2	O9	C15	C14	C13	-66.3(1)
3	O9	C15	C16	C17	43.8(1)
4	C15	C14	C13	O4	-146.3(1)
5	C15	C16	C17	O6	75.6(1)

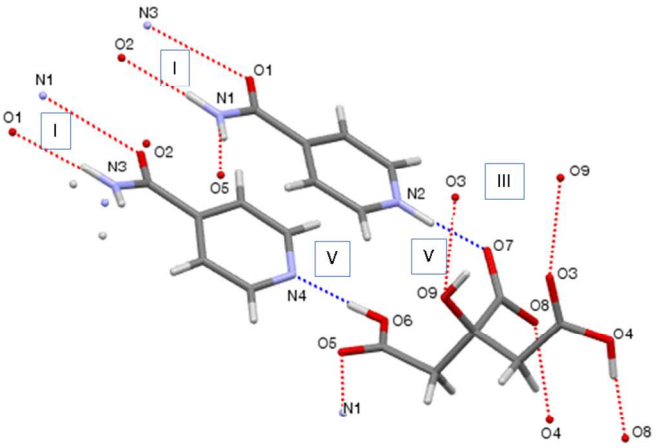

This adds confidence when considering the inspection of torsions and degree of planarity along with positioning of hydrogen based on electron density the molecular complex situation exists for the alpha, beta and gamma, whereas in latter phase (salt) the ionic contact is clearly identified at 07/08 oxygens. (see above).

4. Supporting Computational Analysis

Table S10 - Attachment Energies

Phase	(hkl)	Attachment Energy (kJ/mol)
α	(100)	-235.89
	(001)	-233.01
	(01-1)	-224.29
	(1-10)	-173.30
	(010)	-169.62
	(10-1)	-130.89
β	(110)	-662.20
	(100)	-568.40
	(111)	-541.16
	(011)	-461.33
	(020)	-411.96
γ	(11-1)	-513.71
	(111)	-500.36
	(110)	-463.84
	(002)	-372.46
	(202)	-354.80
	(-200)	-131.21
Salt	(1-11)	-172.51
	(10-1)	-159.28
	(001)	-141.21
	(01-1)	-128.83
	(010)	-121.59
	(100)	-118.87
	(1-10)	-113.14

Table S11 – Lattice Energies

Form	Lattice Energy (kJ/mol)
α	-545.99
β	-1841.28
γ	-861.74
Salt	-382.30

Table S12 - Intermolecular Potentials

Phase	Mol1	Mol2	Distance (Å)	Energy (kJ/mol)
α	CA	CA	5.96603	-37.6322
	CA	IN	5.3796	-31.5209
	IN	IN	7.67121	-30.565
	IN	IN	7.65198	-29.8012
	CA	IN	8.47611	-24.7968
β	CA	CA	5.89886	-35.8708
	CA	IN	5.46314	-33.543
	CA	IN	5.66969	-31.2608
	IN	IN	7.64778	-30.1018
	IN	IN	7.70143	-28.7327
γ	IN	IN	7.58966	-32.0563
	CA	IN	7.6726	-27.6931
	CA	IN	5.98644	-27.0973
	CA	CA	5.3196	-21.7932
	CA	IN	6.48566	-21.5072
Salt	CA	CA	5.61185	-59.4692
	IN	IN	7.7858	-31.6862
	IN	IN	3.73954	-30.7954
	CA	IN	6.05655	-25.7195
	IN	IN	4.13629	-25.5004

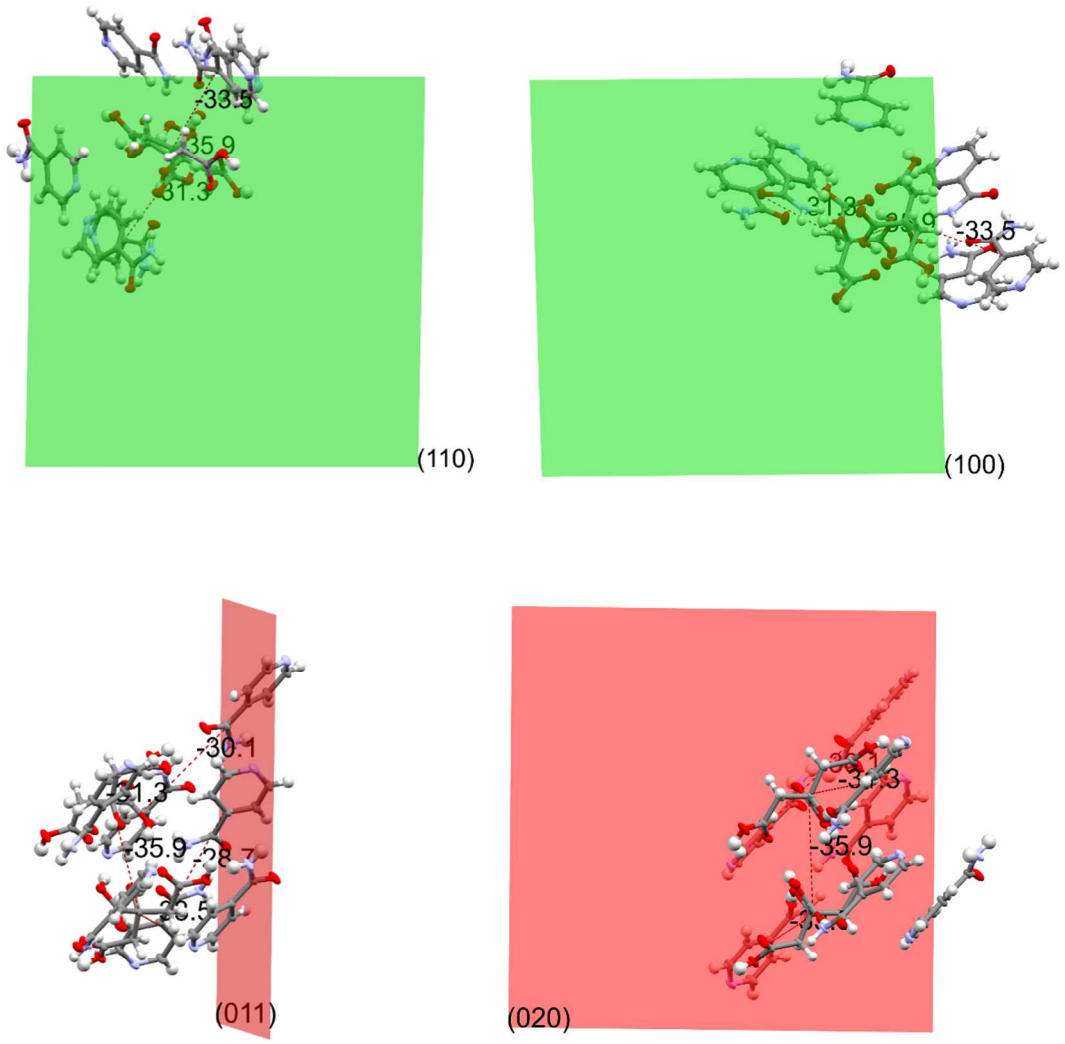

Figure S17 - Calculated intermolecular potentials of β form with slowest growing faces in red and fastest growing faces in green. Fastest face (110) (top left). Second fastest face (100) (top right). Second slowest face (011) (bottom left). Slowest face (020) (bottom right).

The fastest faces in the β form (110) and (100) exhibit easy chain growth directly in the face whereas the slowest face (020) shows the layers are oriented perpendicular to the plane of the face. This makes it difficult for an approaching molecule to integrate into the face make it much less likely. The second slowest face (011) shows growth occurs in directions away from the face therefore growth of this face only occurs by the growth of other faster faces.

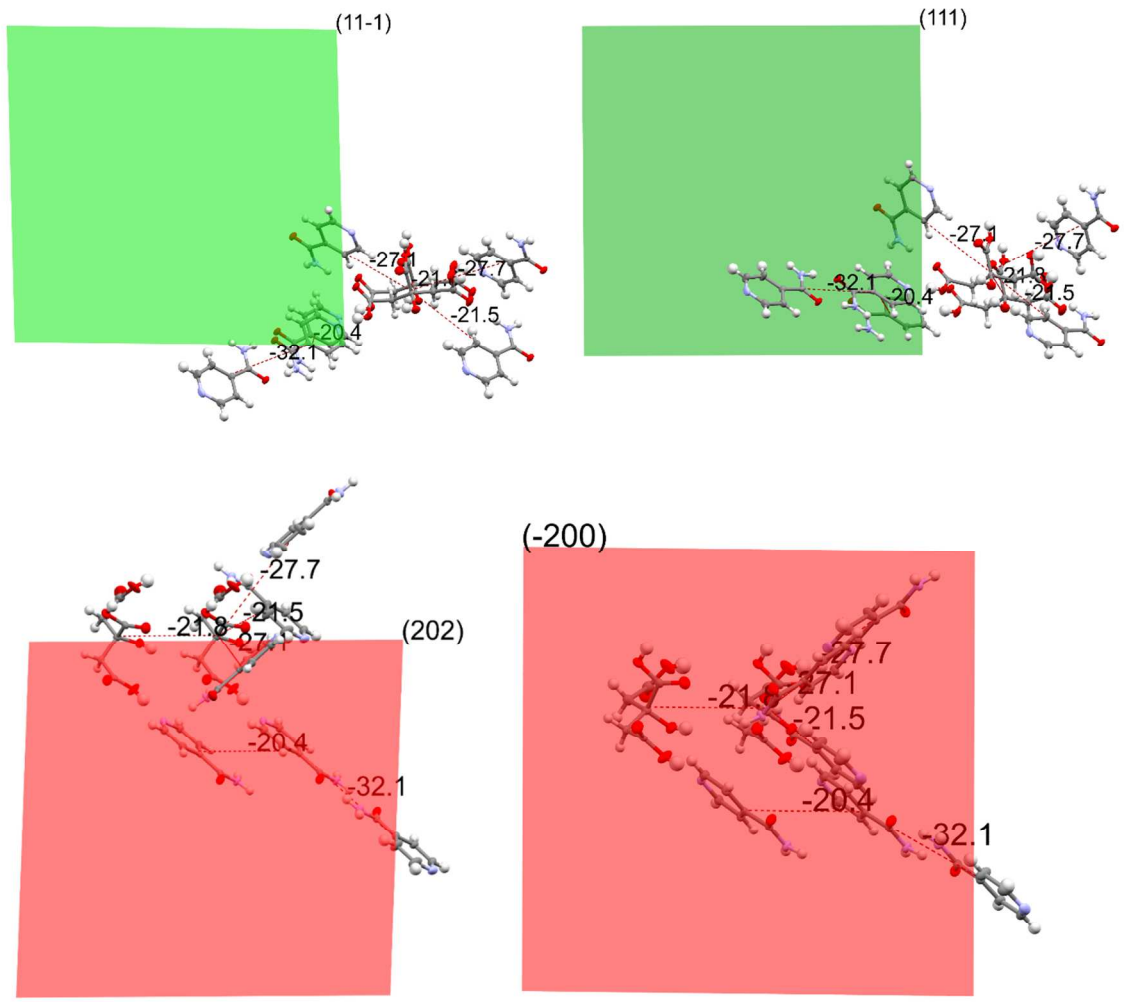

Figure S18 - Calculated intermolecular potentials of γ form with slowest growing faces in red and fastest growing faces in green. Fastest face (11-1) (top left). Second fastest face (111) (top right). Second slowest face (202) (bottom left). Slowest face (-202) (bottom right).

The fastest faces of the γ (11-1) and (111) are the fastest growing faces out of all phases considered. Growth is very easy due to the linear chains and sheets formed in these directions. Single sheets of CA are layered in these directions which are then layered on the top and bottom by IN. The slowest faces (-200) and (202) show that molecules chain growth orients away from these faces where growth of the slower faces is only possible by the growth of the faster faces.

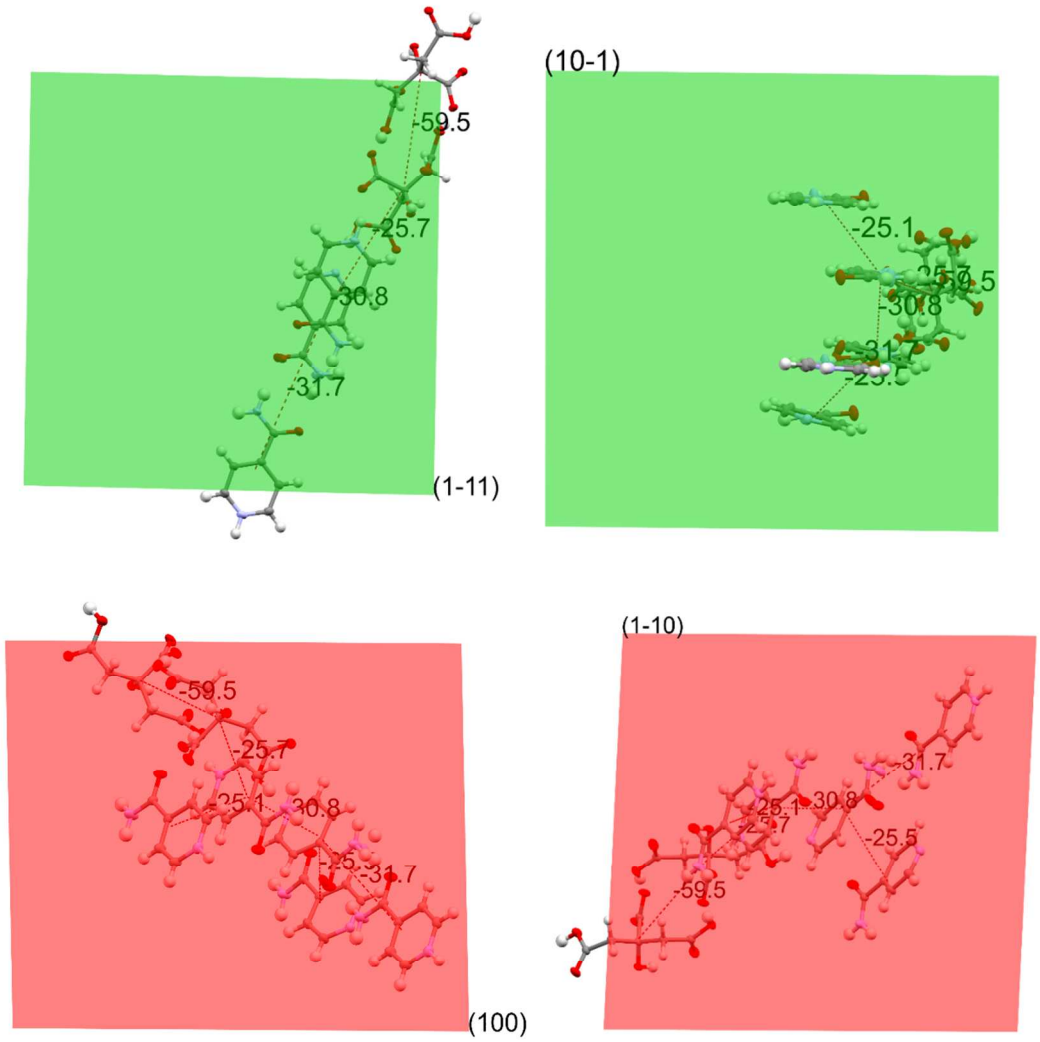

Figure S19 - Calculated intermolecular potentials of salt form with slowest growing faces in red and fastest growing faces in green. Fastest face (1-11) (top left). Second fastest face (10-1) (top right). Second slowest face (100) (bottom left). Slowest face (1-10) (bottom right).

The salt form growth mechanism is very like the α form. The two fastest-growing faces are (1-11) and (10-1) respectively. The fastest face is due to π-π stacking and the second fastest due to ease chain growth with strong intermolecular interactions. Growth of the slowest faces is slow because chain growth occurs away from these faces.

Interaction Mapping

Interaction maps allow a visual representation of the best environment for bonding to occur, to produce the most stable material. Energy differences produced by a molecule create hotspots where when fully occupied by a counter-molecule, are stable. If a molecule occupies the space outside these hotspots then the material is less stable. Interaction mapping allows for estimates in the order of stability of each form by examining these hotspots, and the extent to which they have been occupied.

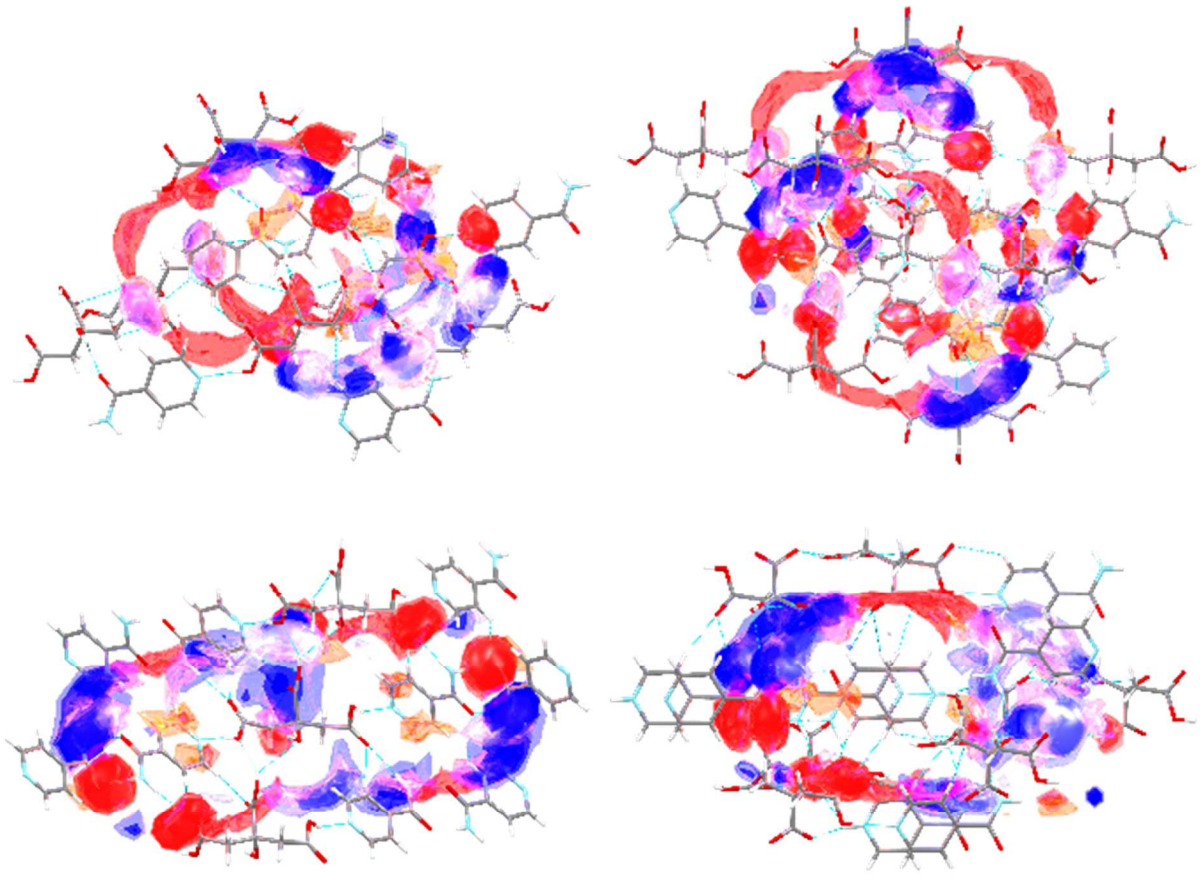

Figure S20 - Interaction maps of α (top left), β (top right), γ (bottom left), salt (bottom right).